Studies on drug development and mechanism for the regulation of helper T cell subsets differentiation

Shunsuke Nomura

2019

Contents

Preface

After recognizing foreign antigens, naive $CD4^+$ T cells differentiate into several effector helper T cell subsets including Th1, Th2, Th17, and iTreg to orchestrate immune response against foreign pathogens. However, they have the potential to drive immune-mediated disease. To development drug of immune-mediated disease, it is important that to uncover the mechanism for the regulation of helper T cell subsets differentiation.

Several transcription factors that control the differentiation of these Th subsets have been identified such as T-bet, Gata3, Rorγt and Foxp3 for Th1, Th2, Th17 and iTreg cells, respectively. Theses transcription factor have been considered an attractive therapeutic target for modulating immune-mediated diseases. However, it remains a challenge to develop an inhibitor against transcription factors.

These transcription factors induced in dependence of antigen and the specific cytokines orchestrates comprehensively gene regulations essential for Th subsets differentiation. Resent studies indicated that these processes highly demand the intracellular energy and intermediate metabolite through glycolysis, mitochondrial oxidative phosphorylation (OXPHOS) and Lipid synthesis. T cells therefore rely on environmental nutrients, including glucose and amino acids. Although inhibition of the nutrients uptakes severely impaired the activation and effector function of T cells, recent studies indicate that distinct metabolic pathways are used for each Th subsets. Therefore, selective modulation of metabolic pathways may permit to ameliorate the inflammation and promote antitumor activity. However, how specific metabolic pathway induces distinct effector T cells remains poorly understood.

In this study, we accessed these problems. In chapter I, we demonstrated that the efficiency of our drug screening system for the development of novel small compounds that inhibit the DNA-binding activity of transcription factors. In chapter II, we presented the

possibility that selective modulation of Gls1-dependent glutaminolysis pathway ameliorates Th17 cell dependent inflammation.

Chapter I

Pyrrothiogatain acts as an inhibitor of GATA family proteins and inhibits Th2 cell differentiation *in vitro*

Summary

The transcription factor GATA3 is a master regulator that modulates T helper 2 (Th2) cell differentiation and induces expression of Th2 cytokines, such as IL-4, IL-5, and IL-13. Th2 cytokines are involved in the protective immune response against foreign pathogens, such as parasites. However, excessive production of Th2 cytokines results in type-2 allergic inflammation. Therefore, the application of a GATA3 inhibitor provides a new therapeutic strategy to regulate Th2 cytokine production. Here, we established a novel high-throughput screening system for an inhibitor of a DNA-binding protein, such as a transcription factor, and identified pyrrothiogatain as a novel inhibitor of GATA3 DNA-binding activity. Pyrrothiogatain inhibited the DNA-binding activity of GATA3 and other members of the GATA family. Pyrrothiogatain also inhibited the interaction between GATA3 and SOX4, suggesting that it interacts with the DNA-binding region of GATA3. Furthermore, pyrrothiogatain significantly suppressed Th2 cell differentiation, without impairing Th1 cell differentiation, and inhibited the expression and production of Th2 cytokines. Furthermore, pyrrothiogatain inhibited the DNA-binding of GATA3 to Th2 cyokine gene locus during Th2 differentiation.

Our results suggest that pyrrothiogatain regulates the differentiation and function of Th2 cells via inhibition of GATA3 DNA binding activity, which demonstrates the efficiency of our drug screening system for the development of novel small compounds that inhibit the DNA-binding activity of transcription factors.

Introduction

Transcription factors are key molecules that regulate gene expression and cell fate in response to cell signalling stimuli from extracellular environments[1,2]. As a final step of multiple signal transductions, transcription factors regulate gene expression via nuclear translocation, dimerization, and DNA binding on the target regulatory regions in the genome. In the case of a pharmacological target of transcription factors, the direct inhibition of these events facilitates drug development[3]. The main biochemical properties of transcription factors are DNA binding and protein-protein interaction. However, it is difficult to establish a drug screening system to generate inhibitors against transcription factors because the recombinant expression and purification of bioactive transcription factors is challenging because, without their partner proteins or target DNA, they generally have an unstable structure[3,4]. In addition, transcription factors, except for the nuclear receptor family, lack a deep hydrophobic pocket that allows access to a small molecular compound which modulates its biological function[4]. Therefore, it remains a challenge to develop an inhibitor against transcription factors, which have been regarded as an efficient target for therapy.

After recognizing foreign antigens, naive $CD4^+$ T cells differentiate into several effector helper T cell subsets including Th1, Th2, Th17, and iTreg, which play key roles in adaptive immune responses; but they have the potential to drive immune-mediated diseases[5,6]. The pathology of allergic asthma, which is a Th2 cytokine-mediated disorder, is characterized by eosinophilia, goblet cell hyperplasia, and airway smooth muscle contraction[7]. These pathological events are due to the excessive differentiation and activation of Th2 cells[8], which are a major source of Th2 cytokines, such as IL-4, IL-5, and IL-13[9]. Therefore, a strategy that modulates the differentiation and function of Th2 cells will lead to a novel therapeutic strategy for allergic disorders.

The GATA (GATA-binding protein) family consists of six members from GATA1 to GATA6. They contain a transactivation domain in the N-terminal region and a zinc-finger DNA-binding domain in the C-terminal region, and bind to the specific DNA sequence (A/T)-GATA-(A/G). GATA3 has been identified as a master regulator that controls Th2 cell differentiation and the production of Th2 cytokines by binding to a broad range of Th2 cytokine gene locus[10,11], whereas GATA3 suppresses Th1 cell differentiation by blocking transcription of Th1-specific genes[12-16]. Among the Th2 cytokine genes, IL-5 and IL-13 are directly regulated by the binding of GATA3 with the corresponding promoter region[5,17]. Importantly, the upregulation of GATA3 has been reported in allergic inflammatory cells in allergy patients[18,19] and is considered an attractive therapeutic target for ameliorating allergic inflammation[8].

In this study, we established a high-throughput inhibitor screening system for transcription factors using GATA3 as a model. The inhibitor screening system specifically identified factors inhibiting the DNA-binding activity of transcription factors and facilitated the development of a novel GATA family inhibitor, pyrrothiogatain. Our results showed pyrrothiogatain inhibited the DNA-binding activity of GATA3. Furthermore, pyrrothiogatain suppressed *in vitro* Th2 cell differentiation and the secretion of Th2 cytokines without impairing Th1 cell differentiation.

Materials and Methods

Plasmid construction

The open reading frame of cDNA clones obtained from the Mammalian Gene Collection was subcloned into the pEU-based expression vector for the wheat cell-free protein synthesis system or into pcDNA3.1 for mammalian cell expression.

Wheat cell-free protein synthesis and immunoblot analysis

In vitro transcription and translation were performed by the bilayer method using the WEPRO1240 expression kit (Cell-Free Sciences), according to the manufacturer's instructions. Biotin labelling was carried out by the method described previously[20]. Specifically, during translation, biotin ligase (BirA), synthesized by a wheat cell-free system, was added to the bottom layer and incubated in the presence of 0.5 μM D-biotin (Nacalai Tesque). The whole lysate and supernatant after its centrifugation were analysed by immunoblotting using anti-FALG-HRP antibody (M2, Cat#A8592, Sigma, 1:4000) and anti-AGIA-HRP[21].

DNA-binding assay using AlphaScreen technology

For the protein-DNA binding assay on a 384-well AlphaPlate (Perkin Elmer), 10 μL of bait protein mixture containing 1 μL FLAG-tagged protein in AlphaScreen Buffer (100 mM Tris-HCl (pH 8.0), 150 mM NaCl, 0.1% Tween 20, and 1 mg/mL BSA) and 5 μL biotinylated oligonucleotide (0 - 10 μM final concentration) in AlphaScreen Buffer were dispended into the AlphaPlate. Then, the plate was incubated at 26°C for 1 h. After incubation, 10 μL of the detection mixture containing 0.4 μg/mL Anti-DYKDDDDK antibody (1E6, Wako), 0.1 μL streptavidin-conjugated AlphaScreen donor beads, and 0.1 μL protein A-conjugated AlphaScreen acceptor beads in AlphaScreen Buffer was mixed

and incubated at 26°C for 1 h, and then, the AlphaScreen signal was detected using an EnVision device with the AlphaScreen signal detection program (PerkinElmer).

The following oligonucleotides were used:

GATA3 consensus DNA, 5'-biotin-CACTTGATAACAGAAAGTGATAACTCT-3';

MT, 5'-biotin-CACTTCTTAACAGAAAGTCTTAACTCT-3'.

Drug screening and validation

All chemical compounds (10 mM) were dissolved in DMSO, and were pre-dispensed into a 384-well Alphaplate (250 nL/well). Ten microliters of bait protein mixture containing 1 μL of FLAG-tagged GATA3 protein in AlphaScreen Buffer was dispensed into the Alphaplate-384 plate (Cat# 6005350) using a FlexDrop dispenser (PerkinElmer), and 5 μL biotinylated DNA (4 nM final concentration) in AlphaScreen Buffer was mixed on the AlphaPlate by the dispenser. Then, the plate was incubated at 26°C for 1 h. After incubation for 1 h, 10 μL of detection mixture was added, followed by further incubation at 26°C for 1 h. The AlphaScreen signal was detected using an EnVision device with the AlphaScreen signal detection program (PerkinElmer). For determination of IC50, the same assays were performed for GATA2 and GATA5 in the presence of various concentration of pyrrothiogatain (0 to 200 μM). The obtained data was fitted using the 4-parameter non-linear regression of GraphPad Prism version 8.0.

Pyrrothiogatain(3-(2,5-dimethyl-1H-pyrrol-1-yl)thiophene-2-carboxylic acid)

Pyrrothiogatain (CAS No.: 477888-48-5) was purchased from Enamine (cat#EN300-5110 4) and Santa Cruz (cat#sc-352288A).Electrophoretic mobility shift assays were performed as described previously22. In brief, four GATA family proteins (GATA2 to GATA5) were incubated with a 32P-labelled GATA-binding DNA probe for 20 min at 4ºC in the presence

or absence of pyrrothiogatain (0 to 100 μM). The DNA-protein complex was separated from free oligonucleotides on 4% polyacrylamide gels, and then, the 32P-labelled DNA probes were detected using the Typhoon FLA 7000 (GE Healthcare).

MTS assay

Jurkat cells were cultured at 37ºC with 5% CO2 in RPMI 1640 Medium (cat#72400047; Thermo Fisher) in the presence or absence of pyrrothiogatain (0 to 100 μM). Cell viability was measured using a CellTiter 96® AQueous One Solution Cell Proliferation Assay (cat#G3582; Promega) according to the manufacturer's protocol.

Luciferase reporter assay

The IL-5 promoter activity was determined as previously described[23,24]. In brief, HEK293T cells were co-transfected with a firefly luciferase reporter (pGL3-IL-5 promoter), a renilla luciferase plasmid, and an expression vector (pcDNA3.1) using TransIT-LTI Regent (Cat#MIR2304, Mirus). Six hours after transfection, cells were treated with pyrrothiogatain (0 to 30 μM) and PMA (30 ng/mL) for 18 hours. The luciferase activity was measured using a Dual-Luciferase Reporter Assay System (cat#E1910, Promega).

Immunoprecipitation

Co-immunoprecipitation analysis of GATA3 and SOX4 was conducted as follows. Immunoprecipitation of FLAG-tagged GATA3 in the presence of pyrrothiogatain (0 to 100 μM) was performed by mixing recombinant FLAG-GATA3 and AGIA-SOX4 with 10 μL of anti-FLAG M2 affinity agarose gel (cat#A2220, Sigma-Aldrich) by rotation at 4ºC for 2 h. The agarose gels were washed three times, and then the immunoprecipitated protein was detected by immunoblotting using anti-FLAG M2 antibody and anti-AGIA-HRP[21].

$CD4^+$ T cell–differentiation cultures

C57BL/6 mice were purchased from Clea (Clea Japan, Inc., Tokyo, Japan). Total $CD4^+$ T cells isolated from mouse spleen were prepared using a FITC anti-mouse CD4 antibody (Cat#100510, RM4-5, BioLegend) and anti-FITC-microbeads (Cat#130-097-050, Miltenyi Biotec). Naive $CD4^+$ T cells ($CD44^{low}$, $CD62L^{high}$) were prepared using a MojoSort Mouse CD4 T cell Isolation Kit (Cat#480033), BioLegend). Biotinylated anti-CD44 (Cat#103004, IM7) and anti-CD25 antibodies (Cat#102004, PC61) were purchased from BioLegend. $CD4^+$ T cells (7.5×10^5) were stimulated using immobilized anti-TCR-β mAb (3 μg/mL, H57-597, BioLegend) plus an anti-CD28 mAb (1.0 μg/mL, cat#40-0281, TONBO Biosciences) for 2 days, and then, the cells were further expanded under similar conditions for an additional 3 days. IL-2 conditions: IL-2 (10 ng/mL, Pepro Tech); Th2 conditions: IL-2 (10 ng/mL, Pepro Tech), IL-4 (1 ng/mL, Pepro Tech), and anti-IFN-γ mAb (2.5 μg/mL, cat#40-731, TONBO Biosciences). Th1 conditions: IL-2 (10 ng/mL, Pepro Tech), IL-12 (1 ng/mL, Pepro Tech), and anti-IL-4 mAb (2.5 μg/mL, cat#40-731, TONBO Biosciences). The cultured cells were subjected to intracellular staining, ELISA assay, and RT-PCR. All animal experiments received approval from the Ehime University Administrative Panel for Animal Care. All animal care was conducted in accordance with the guidelines of Ehime University.

Intracellular staining of cytokines and transcription factors

The *in vitro* differentiated $CD4^+$ T cells were stimulated using an immobilized anti-TCR-β mAb (3 μg/ml, H57–597, BioLegend) for 6 h in the presence of monensin (2 μM). The cells were fixed with 4% paraformaldehyde (Cat#163-20145, Wako) and permeabilized with permeabilization buffer (50 mM NaCl, 5 mM EDTA, 0.02% NaN_3, and 0.5% Triton

X-100). Then, the cells were stained using the following antibodies, anti-IL-4-PE (Cat#504103, BioLegend, 1:50), anti-IL-5-APC (Cat#504305, BioLegend, 1:50), anti-IL-13-PE (Cat#12-7133-41, eBiosience, 1:50), anti-IFN-g-FITC (Cat#562019, BD Biosciences, 1:500), and anti-IL-2-APC (Cat#503809, BioLegend, 1:50). For the intracellular staining of Gata3, the Foxp3/Transcription Factor Staining Buffer Kit (cat#TNB-0607, TONBO) was used according to the manufacturer's protocol. Flow cytometry was performed using a Gallios Flow Cytometer instrument (Beckman Coulter) and a FACS Caliber instrument (BD Biosciences) and the results were analysed using the FlowJo software program (Tree Star, Ashland, OR, USA).

ELISA assay

The $CD4^+$ T cells cultured for five days were stimulated using an immobilized anti-TCR-β mAb (3 μg/mL, H57-597, BioLegend) for 16 h, and the culture supernatants were recovered. The amount of cytokines in the recovered supernatants was determined with ELISA using the following antibodies and reagents: anti-IL-4 mAb (Cat#554387, BD Biosciences), biotin-anti-IL-4 mAb (Cat#554390, BD Biosciences), anti-IL-5 mAb (Cat#554393, BD Biosciences), biotin-anti-IL-5 mAb (Cat#554397, BD Biosciences), anti-IFN-γ mAb (Cat#551216, BD Biosciences), biotin-anti-IFN-γ mAb (Cat#554410, BD Biosciences), anti-IL-2 mAb (Cat#554424, BD Biosciences), biotin-anti-IL-2 mAb (Cat#554426, BD Biosciences), streptavidin horseradish peroxidase (Cat#434323, Invitrogen), and TMB peroxidase EIA substrate kit (Cat#1721066, BioRad). For IL-13, the mouse IL-13 Duoset ELISA (Cat#DY413, R&D systems) was used for detecting the levels of the IL-13 cytokine. All antibodies and reagents were used according to the manufacturer's protocols.

Quantitative RT-PCR

Total RNA was isolated using the TRI Reagent (Molecular Research Center, Inc.). Reverse transcription and qRT-PCR were performed using the Transcriptor First Strand cDNA Synthesis Kit (Cat#04379012001, Roche) and FastStart Essential DNA Green Master (Cat#06402712001, Roche), according to the manufacturer's protocols. qRT-PCR primers were used as follow; IL-4: 5'-GATCGGCATTTTCAACGAG-3' (forward), 5'-CGAGCTCACTCTCTGTGGTG-3' (reverse); IL-13: 5'-ACCCAGAGGATATTGCATGG-3' (forward), 5'-TGGGCTACTTCGATTTTGGT-3' (reverse); IFN-γ: 5'-ATCTGGAGGAACTGGCAAAA-3' (forward), 5'-TTCAAGACTTCAAAGAGTCTGAGGTA-3' (reverse); IL-2: 5'-GCTGTTGATGGACCTACAGGA-3' (forward), 5'-TTCAATTCTGTGGCCTGCTT-3' (reverse); Gata3: 5'-TTATCAAGCCCAAGCGAAG-3' (forward), 5'-TGGTGGTGGTCTGACAGTT-3' (reverse); and Tbx21: 5'-TCAACCAGCACCAGACAGAG-3' (forward), 5'-AAACATCCTGTAATGGCTTGTG-3' (reverse).

Chromatin immunoprecipitation assay

The Magna ChIP Chromatin Immunoprecipitation Kit was used for the ChIP assay according to the manufacturer's protocol (Merck-Millipore). Anti-GATA3 antibody (Cat#AF2605, R&D systems) was used for chromatin immunoprecipitation. The specific primers for the Th2 cytokine gene locus and the Roche Universal probes were used as follows: the V_A site in the IL-4 enhancer: 5'-GCCTGTTTCCTCTCAGCATT-3' (forward), 5'-TGATAAAAGTGACTTGAAGGTTGG-3' (reverse), probe #4; IL-4 IE: 5'-CCCAAAGGAGGTGCTTTTATC-3' (forward), 5'-AAATCCGAAACTGA GGAGTGC-3' (reverse), probe #75; CGRE: 5'-CTCTCCTGGTGGCGTGTT-3' (forward),

5’-CTTTGCGCACCCTTGAAC-3’ (reverse), probe #53; and IL-5p: 5’-TCACTTTATCAGGAATTGAGTTTAACA-3’ (forward), 5’-GATCGGCTTTTCTTGAGCAC-3’ (reverse), probe #43;

OVA-induced allergic airway inflammation model

C57BL/6 mice at 7 weeks old were immunized intraperitoneally with 100 μg OVA (Cat#A5503, Sigma) in 2 % aluminium hydroxide gel (Cat#vax-alu-250, InvivoGen) on day 0. The mice were challenged intranasally with 100 μg OVA in saline on days 7, 8 and 9. Pyrrothiogatain was administrated intraperitoneally at a concentration of 20 mg/kg in PBS every day from day 0 to 6. The day after the last OVA challenge, BAL fluid cells were subjected to histological examination using the Diff Quick stain (Cat#16920, Sysmex). All animal experiments received approval from the Ehime University Administrative Panel for Animal Care. All animal care was conducted in accordance with the guidelines of Ehime University.

Statistical analysis and number of replicates per experiments

Statistical significance was calculated using two-tailed unpaired Student’s t-test (Microsoft Excel, USA). Statistical significance was accepted at $p < 0.05$. All *in vitro* assays were repeated at least three times.

Results

Establishment of a high-throughput assay to detect a DNA–protein interaction

Previously, we developed a drug screening system to generate an inhibitor against a protein-protein interaction based on a wheat cell-free system and AlphaScreen technology[22,25], which is a high-throughput luminescence-based binding assay. We identified an NF-κB inhibitor (DANFIN)[22] and two agonists for abscisic acid receptor (JFA1 and JFA2)[25]. In this study, we attempted to construct a drug screening system for the development of inhibitors against a DNA-protein interaction using the cell-free based system. As a model, we selected the GATA3 transcription factor because GATA3 is known as the master regulator for Th2 cell differentiation and production of Th2 cytokines[10,11] and GATA3-binding to its DNA sequence has already been reported[11]. To determine the functions of the GATA3 protein, we synthesized the recombinant full-length GATA3 protein with an N-terminal FLAG tag using the wheat cell-free system. The levels of GATA3 in the whole translational mixture (W) and the supernatant (S), obtained after centrifugation of the former, were determined by immunoblot analysis (Fig. 1A), indicating that the recombinant full-length GATA3 was synthesized as a soluble form.

We used AlphaScreen technology[22,25] to detect the direct binding between GATA3 and its target DNA (TGATAA) labelled with biotin (Fig. 1B). We performed the binding assay using recombinant FLAG-tagged full-length GATA3 and the biotinylated GATA-consensus DNA (GATA DNA) or the negative control DNA mutated in the GATA-binding motif (mutant DNA) under various NaCl concentrations (100 to 150 mM). A high luminescence signal was obtained by the binding between GATA3 and the target DNA (Fig. 1C). A considerable luminescence signal due to non-specific binding of GATA3 with the negative control DNA was also observed in the presence of 100 mM and 125 mM NaCl, whereas the luminescence signal of the negative control was disrupted in the

presence of 150 mM NaCl. In addition, the binding assay was performed under various concentrations of GATA DNA, for which the luminescence signal intensified in a dose-dependent manner (Fig. 1D). In contrast, the negative control DNA produced a luminescence signal (<1500) of very low intensity comparable to the background intensity level. These results indicated that this binding system could detect the interaction between specific DNA and the GATA3 protein.

To further validate whether the binding assay could detect the inhibition of the interaction between biotinylated DNA and the GATA3 protein, a competition assay was performed using supplementary non-labelled DNA with the same sequence. As a result, a dose-dependent decrease in the intensity of the luminescence signal was observed by supplementation with non-labelled GATA consensus DNA (Fig. 1E). In contrast, the DNA binding activity of GATA3 was not influenced by mutant DNA supplementation. These results suggested that this assay could detect the inhibition of the GATA3–DNA interaction.

Next, we investigated whether the assay was suitable for high-throughput screening by 20-independent positive reactions and negative reactions, and a Z' factor, known as indicator of the accuracy and quality of high-throughput screening, that was calculated for the validation. The Z' factor was found to be 0.88, indicating that this cell-free assay for the protein-DNA interaction could be used for high-throughput screening.

Identification of a GATA3 inhibitor using the wheat cell-free drug screening system

We performed high-throughput screening using the assay shown in Fig. 1 to identify inhibitors of GATA3 DNA binding activity. The results of drug screening are summarized as a flow chart in Fig. 2A. We identified 105 candidate compounds that showed an inhibition rate > 20% at a compound concentration of 10 μM in the first screening of 9,600

compounds (Fig. 2B). We performed a second screen to exclude the false-positive compounds. As shown in Fig. 2C, one compound was identified that specifically inhibited GATA3–DNA binding without interfering with both the AlphaScreen assay and the RelA-DNA interaction. We identified this compound (3-(2,5-dimethyl-1H-pyrrol-1-yl)thiophene-2-carboxylic acid) as a pyrrothiogatain (pyrrole and thiofuran containing GATA3 inhibitor) (Fig. 2A). The inhibitory activity of pyrrothiogatain for the GATA3-DNA interaction was validated by electrophoretic mobility shift assay (EMSA). The intensity of the shifted bands generated by GATA3-DNA binding was decreased in a pyrrothiogatain dose-dependent manner (50 to 100 μM) (Fig. 2D), indicating that pyrrothiogatain inhibited the GATA3–DNA interaction.

Next, cytotoxicity was performed to assess whether pyrrothiogatain could be used in a cell-based assay. Jurkat cells were cultured in the presence of various concentrations of pyrrothiogatain (0 to 100 μM) for 3 days and cell viability was determined by MTS assay. As shown in Fig. 2E, pyrrothiogatain did not influence cell viability. GATA3 induces the transcription of the *IL-5* gene through the direct binding of the GATA consensus motif on the IL-5 promoter[5]. We therefore investigated whether pyrrothiogatain inhibited GATA3-dependent IL-5 promoter activation using a luciferase reporter assay with the IL-5 promoter[23,24]. As shown in Fig. 2F, pyrrothiogatain significantly suppressed GATA3-dependent transcriptional activation of the IL-5 promoter, suggesting that pyrrothiogatain inhibited DNA binding activity of GATA3 in the cells. Taken together, these results indicated that pyrrothiogatain, obtained from the wheat cell-free based screening, inhibited the function of GATA3.

Effect of pyrrothiogatain on the DNA-binding activity of other GATA family proteins

We next assessed the inhibitory effect of pyrrothiogatain on the DNA-binding activities of other GATA family proteins using the cell-free system and AlphaScreen technology. Six GATA proteins from GATA1 to GATA6 have been reported[11], and we tried to synthesize their full-length proteins using the cell-free system. GATA proteins, except for GATA6, were successfully synthesized as a soluble form (Fig. 3A), and four GATA proteins, GATA2 to GATA5, exhibited comparable DNA-binding activity (Fig. 3B). Since the GATA1 protein did not bind to the same DNA probe, it was excluded from further analysis. Pyrrothiogatain inhibited the DNA-binding activity of GATA2 to GATA5 (Fig. 3C), with an approximate IC50 value of 50 μM. Similar inhibitory results were obtained by EMSA (Fig. 3D). These data suggest that pyrrothiogatain acts as a pan-inhibitor of GATA family proteins.

Pyrrothiogatain inhibited the GATA3-SOX4 interaction

The GATA3 protein has been reported to directly interact with SOX4[23]. We next investigated whether pyrrothiogatain interrupted the interaction between GATA3 and SOX4. As shown in Fig. 4A, an immunoblotting analysis revealed that an N-terminal biotinylated full-length SOX4 protein was synthesized by the wheat cell-free system. Interaction between biotin-labelled SOX4 and FLAG-GATA3 was analysed by the AlphaScreen system (Fig. 4B). The interaction indicated that biotinylated SOX4 directly interacted with FLAG-GATA3 (Fig. 4C), but not with FLAG-DHFR, a negative control. A pyrrothiogatain dose-dependent decrease in GATA3-SOX4 interaction was detected using AlphaScreen (Fig. 4D) and immunoprecipitation (Fig. 4E). These results suggested that pyrrothiogatain also inhibited the protein-protein interaction of GATA3.

Pyrrothiogatain inhibited Th2 cell differentiation and the production of Th2 cytokines

It is well established that GATA3 induces Th2 cell differentiation[11]. Since pyrrothiogatain exhibited no effect on the viability of Jurkat T cells (Fig. 2D), we investigated whether pyrrothiogatain inhibited Th2 cell differentiation. Total $CD4^+$ T cells were isolated and cultured under IL-2 conditions in the presence or absence of pyrrothiogatain for five days, and then the Th2 cell differentiation status was determined using intracellular staining. The generation of IL-4-, IL-5-, and IL-13-producing cells was repressed by the treatment of pyrrothiogatain (Supplementary Fig. 1A), whereas the number of Th1 cells producing IFN-γ was increased. In addition, decreased production and mRNA expression of IL-4, IL-5, IL-10, and IL-13 were confirmed using ELISA (Supplementary Fig. 1B) and RT-qPCR (Supplementary Fig. 1C). Increased production and mRNA expression of IFN-γ were also detected. The expression of GATA3 was not influenced at either the mRNA or protein level (Supplementary Fig. 1C and 1D). A previous report indicated that GATA3 may silence the expression of *Tbx21*, a master regulator of Th1 cells, by directly binding the *Tbx21* locus[16]. As expected, the expression of *Tbx21* was increased after treatment with pyrrothiogatain (Supplementary Fig. 1C).

To clarify the effects of pyrrothiogatain on Th2 cell differentiation, naive CD4 T cells were purified and cultured under Th2 conditions in the presence or absence of pyrrothiogatain for 5 days, and then the Th2 cell differentiation status was determined by intracellular staining. The generation of IL-4-, IL-5-, and IL-13-producing Th2 cells was repressed by treatment with pyrrothiogatain. Decreased production and mRNA expression of IL-4, IL-5 and IL-13 were confirmed using ELISA and RT-qPCR, respectively. However, the expression of GATA3 was not influenced at either the mRNA or protein level (Fig. 5C and 5D). The generation of IFN-γ and IL-2 producing Th1 cells under Th1 conditions was modestly increased by treatment with pyrrothiogatain (supplementary Figure 2A and 2B). These results indicated that pyrrothiogatain selectively inhibited Th2

cell differentiation. Next, we treated *in vitro* differentiated Th2 cells with pyrrothiogatain to test the effect of pyrrothiogatain on Th2 cytokine production. Total $CD4^+$ cells were cultured under Th2 conditions for 5 days, and then the Th2 cells were restimulated in the presence or absence of pyrrothiogatain for 16 h. As shown in Figure 5E, IL-4, IL-5 and IL-13 production was decreased by pyrrothiogatain treatment. Finally, we investigated the effects of the administration of pyrrothiogatain in a mouse model of OVA-induced type 2 airway inflammation. We expected that pyrrothiogatain might exhibit a positive therapeutic effect against Th2-dependent allergic inflammation. However, the administration of pyrrothiogatain did not significantly decrease the number of inflammatory cells in the bronchoalveolar lavage (BAL) fluid of OVA-induced allergic mice (Supplementary Fig. S3A and S3B).

Taken together, these results indicated that pyrrothiogatain inhibited Th2 cell differentiation and the production of Th2 cytokines *in vitro*, without influencing the expression of GATA3.

Pyrrothiogatain inhibited GATA3 binding to Th2 cytokine gene locus.

GATA3 has been reported to bind to Th2 cytokine gene locus, such as IL-4 V_A enhancer[26], IL-4 intron enhancer[27], conserved Gata3-response element (CGRE) [28] and IL-5 promoter[29] regions in Th2 cells. We investigated whether pyrrothiogatain inhibited GATA3 binding to Th2 cytokine gene locus. Naive $CD4^+$ T cells were cultured under Th2 conditions in the presence or absence of 80 μM pyrrothiogatain for 2 days, and then the cells were subjected to chromatin immunoprecipitation with an anti-GATA3 antibody. As shown in Figure 6A, pyrrothiogatain repressed GATA3 binding to the IL-4 V_A enhancer, IL-4 intron enhancer, CGRE and IL-5 promoter regions. These results indicated that pyrrothiogatain inhibited GATA3 DNA-binding to Th2 cytokine gene locus in Th2 cells.

Discussion

In this study, we established a drug screening system for the development of inhibitors against transcription factors using a cell-free based system. Although several studies have reported the development of various high-throughput inhibitor screens targeting transcription factors[30-32], our screening system exhibited several advantages. In many cases of pharmacological targeting of transcription factors, methodological problems arise during both the biochemical and cell-based assays. In the case of the biochemical assay, it is difficult to purify transcription factors with DNA-binding activity and to validate that activity with several compounds to determine their biochemical function[3,4], because many transcription factors harbour unstable structural regions without their partner protein or target DNA[4]. In addition, the GATA3 DNA-binding domain contains a flexible linker with an unstructured region[33]. For cell-based drug screening against transcription factors, a luciferase-reporter assay-based screen has been employed with transcriptional activity as an indicator[32]. However, cell-based assays have a high possibility of developing unexpected compounds, indirectly influencing the function of transcription factors[3]. Our wheat cell-free drug screening system does not demand protein purification and makes it possible to detect the DNA-binding activity of transcription factors directly. Therefore, our screening system is useful for the development of chemical compounds targeting transcription factors.

Using the newly developed screening system, we identified pyrrothiogatain, which inhibited the DNA-binding activity of GATA3, from a chemical library of 9,600 small compounds. Pyrrothiogatain suppressed Th2 cell differentiation and production of Th2 cytokines without any influence on GATA3 expression at the mRNA and protein levels (Fig. 5C and 5D). During Th1 cell differentiation, GATA3 is known to repress IFN-γ production and Th1-specific gene expression[12-16]. Since pyrrothiogatain promoted gene expression and production of IFN-g (Supplementary Fig. 1A to 1C), these results also

strongly suggested the inhibition of GATA3 function in cells. In addition, genome-wide analysis of GATA3-binding sites indicates that GATA3 may be involved in silencing of *Tbx21* expression by directly binding the *Tbx21* locus[16]. Our results showed that the *Tbx21* expression was induced after treatment with pyrrothiogatain (Supplementary Fig. 1C). Therefore, these results indicated that pyrrothiogatain acts as a regulatory compound against Th-subset differentiation and inhibits Th2 cell differentiation, which simultaneously leads to Th1 cell differentiation.

GATA3 has been reported to bind to Th2 cytokine gene locus, such as the IL-4 V_A enhancer[26], IL-4 intron enhancer[27] and CGRE[28]. The IL-4 V_A enhancer and IL-4 intron enhancer are regulatory regions for IL-4 production as GATA3 binding sites. In addition, the CGRE is important to induce IL-13 production via GATA3 binding. In this study, we confirmed that pyrrothiogatain suppressed GATA3 binding to these Th2 cytokine gene regions. The result indicated the pyrrothiogatain inhibited Th2 cell differentiation via repression of GATA3 binding to Th2 cytokine gene locus in cells.

As a GATA3 inhibitor targeting mRNA, the DNA enzyme (DNAzyme) cleaving GATA3 mRNA, has been developed for therapy of allergic asthma[34,35]. We expected that pyrrothiogatain might exhibit a positive therapeutic effect against Th2-dependent allergic inflammation. However, the administration of pyrrothiogatain did not significantly decrease the number of inflammatory cells in the bronchoalveolar lavage (BAL) fluid of OVA-induced allergic mice (Supplementary Figure S3A and S3B). This result indicated that pyrrothiogatain is required to improve the inhibitory activity, affinity to GATA3 and/or bioavailability to ameliorate Th2-dependent allergic inflammation.

We investigated whether pyrrothiogatain exhibited inhibitory effects against the DNA-binding activity of GATA family proteins. AlphaScreen and EMSA analysis showed that pyrrothiogatain suppressed the DNA-binding activity of GATA2-GATA5. These

results indicated that pyrrothiogatain influenced the DNA-binding domain of the GATA family, since the DNA-binding domain shows high homology of amino acid sequence among the GATA family. In addition, pyrrothiogatain also inhibited the interaction between GATA3 and SOX4, possibly via interaction with the DNA-binding domain of GATA3[23]. Although the inhibitory effects of pyrrothiogatain could not be evaluated against the DNA-binding activity of GATA1 and GATA6, our experimental results indicated a possibility that pyrrothiogatain inhibited the DNA-binding activity of all GATA family proteins.

The overexpression and dysfunction of transcription factors lead to several human diseases, such as cancer and autoimmune diseases[1]. Therefore, identification of a transcription factor that regulates cell differentiation and fate through regulation of gene expression could be considered as a potential pharmacological target[36]. Instead of controlling transcription factors, regulation of gene expression has also been performed as a therapeutic strategy through the inhibition of upstream signal transduction. However, the pharmacological strategy targeting the signal transducing protein exhibits a lack of specificity and has the potential to generate off-target harmful events[3]. Therefore, development of the drugs directly interacting with transcription factors seems an important issue. In summary, we developed the wheat cell-free drug screening system suitable for development of inhibitors against the DNA-binding activity of transcription factors. Our drug screening system led to the development of a GATA family inhibitor pyrrothiogatain, which regulates Th-subset differentiation, indicating the efficiency of our drug screening system for the development of novel small compounds that inhibit the DNA-binding activity of transcription factors.

References

1. Lee, T. I. & Young, R. A. Transcriptional regulation and its misregulation in disease. *Cell* **152,** 1237–1251 (2013).
2. Singh, H., Khan, A. A. & Dinner, A. R. Gene regulatory networks in the immune system. *Trends Immunol.* **35,** 211–218 (2014).
3. Fontaine, F., Overman, J. & ois, M. F. Pharmacological manipulation of transcription factor protein-protein interactions: opportunities and obstacles. *Cell Regeneration* **4,** 4:2 (2015).
4. Koehler, A. N. A complex task? Direct modulation of transcription factors with small molecules. *Curr Opin Chem Biol* **14,** 331–340 (2010).
5. Zhu, J., Yamane, H. & Paul, W. E. Differentiation of effector CD4 T cell populations (*). *Annu. Rev. Immunol.* **28,** 445–489 (2010).
6. O'Shea, J. J. & Paul, W. E. Mechanisms underlying lineage commitment and plasticity of helper CD4+ T cells. *Science* **327,** 1098–1102 (2010).
7. Adcock, I. M. New targets for drug development in asthma. *Lancet* **372,** 1073–1087 (2008).
8. Bosnjak, B., Stelzmueller, B., Erb, K. J. & Epstein, M. M. Treatment of allergic asthma: modulation of Th2 cells and their responses. *Respir. Res.* **12,** 114 (2011).
9. Walker, J. A. & McKenzie, A. N. J. TH2 cell development and function. *Nature Publishing Group* **18,** 121–133 (2018).
10. Zheng, W. & Flavell, R. A. The transcription factor GATA-3 is necessary and sufficient for Th2 cytokine gene expression in CD4 T cells. *Cell* **89,** 587–596 (1997).
11. Tindemans, I., Serafini, N., Di Santo, J. P. & Hendriks, R. W. GATA-3 function in innate and adaptive immunity. *Immunity* **41,** 191–206 (2014).

12. Yagi, R., Zhu, J. & Paul, W. E. An updated view on transcription factor GATA3-mediated regulation of Th1 and Th2 cell differentiation. *Int. Immunol.* **23,** 415–420 (2011).

13. Kanhere, A. *et al.* T-bet and GATA3 orchestrate Th1 and Th2 differentiation through lineage-specific targeting of distal regulatory elements. *Nat Commun* **3,** 1268 (2012).

14. Usui, T., Nishikomori, R., Kitani, A. & Strober, W. GATA-3 Suppresses Th1 Development by Downregulation of Stat4 and Not through Effects on IL-12Rβ2 Chain or T-bet. *Immunity* **18,** 415–428 (2003).

15. Yagi, R. *et al.* The transcription factor GATA3 actively represses RUNX3 protein-regulated production of interferon-gamma. *Immunity* **32,** 507–517 (2010).

16. Wei, G. *et al.* Genome-wide analyses of transcription factor GATA3-mediated gene regulation in distinct T cell types. *Immunity* **35,** 299–311 (2011).

17. Kishikawa, H., Sun, J., Choi, A., Miaw, S. C. & Ho, I. C. The Cell Type-Specific Expression of the Murine IL-13 Gene Is Regulated by GATA-3. *The Journal of Immunology* **167,** 4414–4420 (2001).

18. Nakamura, Y. *et al.* Gene expression of the GATA-3 transcription factor is increased in atopic asthma. **103,** 215–222 (1999).

19. Larché, M., Robinson, D. S. & Kay, A. B. The role of T lymphocytes in the pathogenesis of asthma. *Journal of Allergy and Clinical Immunology* **111,** 450–463 (2003).

20. Takahashi, H. *et al.* Establishment of a Wheat Cell-Free Synthesized Protein Array Containing 250 Human and Mouse E3 Ubiquitin Ligases to Identify Novel Interaction between E3 Ligases and Substrate Proteins. *PLoS ONE* **11,** e0156718 (2016).

21. Yano, T. *et al.* AGIA Tag System Based on a High Affinity Rabbit Monoclonal Antibody against Human Dopamine Receptor D1 for Protein Analysis. *PLoS ONE* **11,** e0156716 (2016).

22. Uematsu, A. *et al.* DANFIN functions as an inhibitor of transcription factor NF-κB and potentiates the antitumor effect of bortezomib in multiple myeloma. *Biochem. Biophys. Res. Commun.* **495,** 2289–2295 (2018).

23. Kuwahara, M. *et al.* The transcription factor Sox4 is a downstream target of signaling by the cytokine TGF-β and suppresses TH2 differentiation. *Nature Immunology* **13,** 778–786 (2012).

24. Suzuki, J. *et al.* A novel small compound SH-2251 suppresses Th2 cell-dependent airway inflammation through selective modulation of chromatin status at the Il5 gene locus. *PLoS ONE* **8,** e61785 (2013).

25. Nemoto, K. *et al.* Identification of new abscisic acid receptor agonists using a wheat cell-free based drug screening system. *Sci Rep* **8,** 4268 (2018).

26. Agarwal, S., Avni, O. & Rao, A. Cell-type-restricted binding of the transcription factor NFAT to a distal IL-4 enhancer in vivo. *Immunity* **12,** 643–652 (2000).

27. Tanaka, S. *et al.* The enhancer HS2 critically regulates GATA-3-mediated Il4 transcription in T(H)2 cells. *Nature Immunology* **12,** 77–85 (2011).

28. Yamashita, M. *et al.* Identification of a conserved GATA3 response element upstream proximal from the interleukin-13 gene locus. *J. Biol. Chem.* **277,** 42399–42408 (2002).

29. Schwenger, G. T. *et al.* GATA-3 has dual regulatory functions in human interleukin-5 transcription. *J. Biol. Chem.* **276,** 48502–48509 (2001).

30. Narasimhan, K. *et al.* Identification of a polyoxometalate inhibitor of the DNA binding activity of Sox2. *ACS Chem. Biol.* **6,** 573–581 (2011).

31. Altschuler, S. E., Croy, J. E. & Wuttke, D. S. A small molecule inhibitor of Pot1 binding to telomeric DNA. *Biochemistry* **51,** 7833–7845 (2012).

32. Yu, L. *et al.* Reducing Inflammatory Cytokine Production from Renal Collecting Duct Cells by Inhibiting GATA2 Ameliorates Acute Kidney Injury. *Mol. Cell. Biol.* **37,** (2017).

33. Chen, Y. *et al.* DNA binding by GATA transcription factor suggests mechanisms of DNA looping and long-range gene regulation. *Cell Rep* **2,** 1197–1206 (2012).

34. Sel, S. *et al.* Effective prevention and therapy of experimental allergic asthma using a GATA-3-specific DNAzyme. *J. Allergy Clin. Immunol.* **121,** 910–916.e5 (2008).

35. Krug, N. *et al.* Allergen-induced asthmatic responses modified by a GATA3-specific DNAzyme. *N. Engl. J. Med.* **372,** 1987–1995 (2015).

36. Papavassiliou, K. A. & Papavassiliou, A. G. Transcription Factor Drug Targets. *J. Cell. Biochem.* **117,** 2693–2696 (2016).

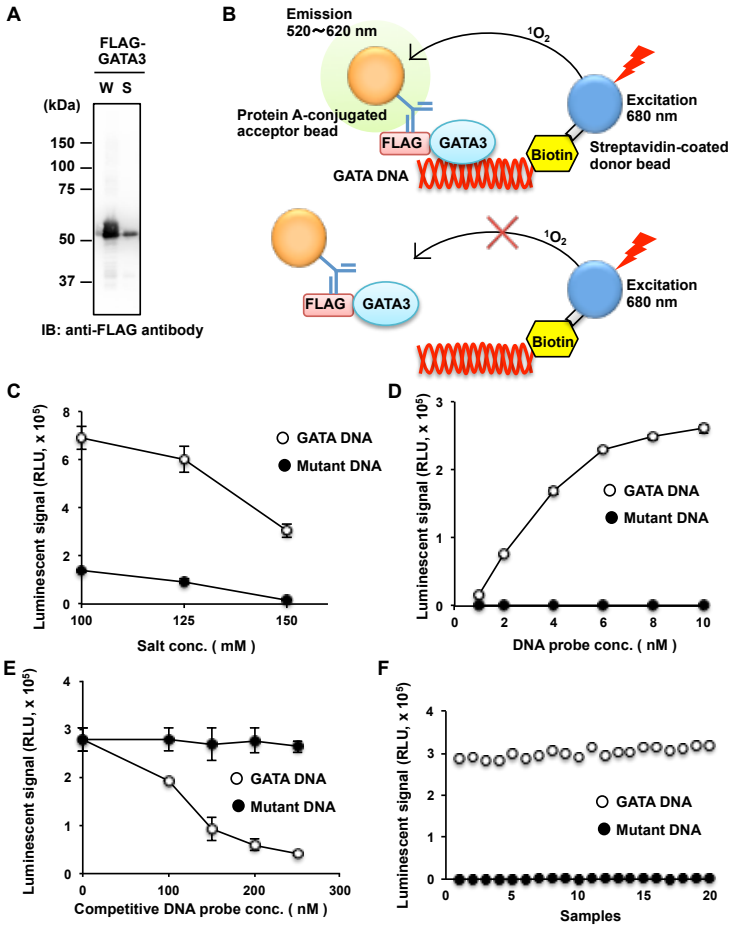

Figure 1 Establishment of the high-throughput assay system to directly detect a DNA–protein interaction

(A) Immunoblot analysis of FLAG-tagged recombinant GATA3 (FLAG-GATA3) synthesized by the wheat cell-free system. The whole translational mixture (W) and the supernatant (S), obtained after centrifugation, were analysed using anti-FLAG M2 antibody. **(B)** A schematic diagram of the high-throughput biochemical DNA-binding assay system to detect the direct binding between GATA3 and its target DNA. When FLAG-tagged GATA3 binds the DNA labelled with biotin at the 5 prime-terminal, AlphaScreen beads generate luminescent signal. **(C)** The binding assay of GATA3 with its consensus DNA-binding motif. The binding assay between the crude translation mixture of FLAG-tagged GATA3 (1 µL) and biotinylated DNA (10 µM) was performed in the presence of various concentrations of NaCl (100 to 150 mM). An oligonucleotide with a mutated GATA-binding site was used as control for this assay. **(D)** The binding assay as described in (C) was performed in the presence of indicated concentrations of biotinylated DNA. A reaction mixture containing FLAG-tagged GATA3 and 150 mM NaCl prepared under the same conditions as those in (C) was mixed with 1 to 10 µM biotinylated DNA. **(E)** Competition assay with non-labelled GATA consensus DNA. The binding assay with the same conditions as those in (D) was mixed with biotinylated DNA (4 µM) and non-labelled GATA consensus DNA (0 to 250 µM) as a control. **(F)** Validation of the quality of the binding assay using AlphaScreen. The 'Z' factor was calculated from the binding reaction of GATA3 with the GATA consensus DNA (positive control, n = 20) or its GATA-binding site mutant (negative control, n = 20). In (C), (D) and (E), all data are expressed as individual points of three independent experiments with error bars indicating standard deviation.

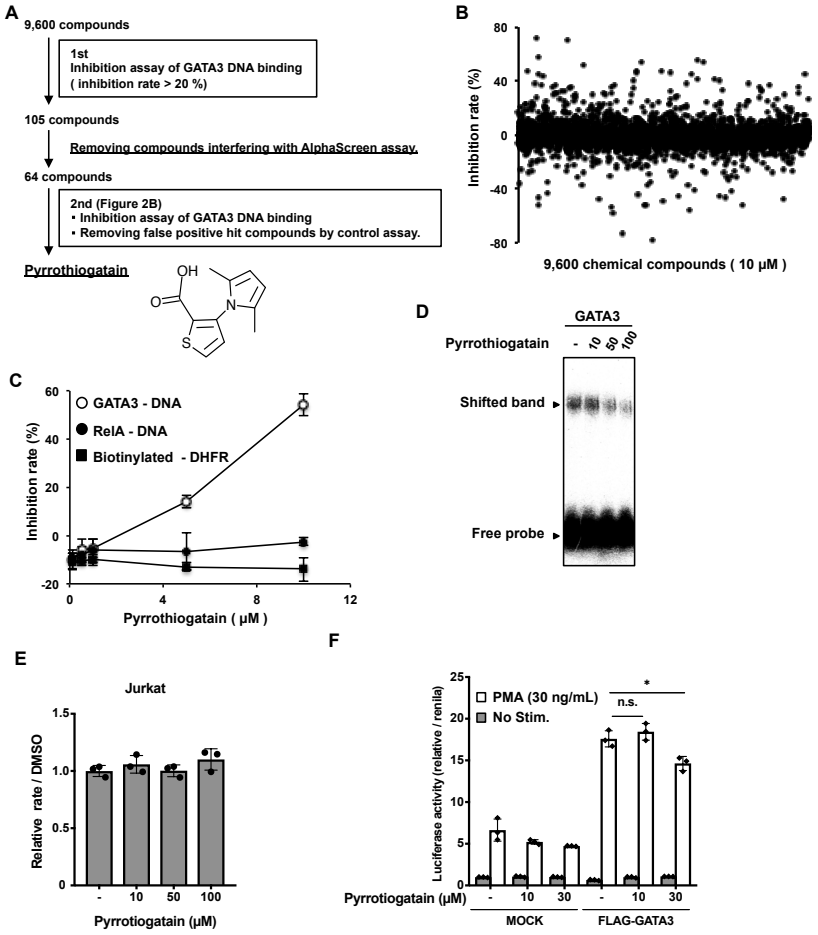

Figure 2 Identification of a GATA3 inhibitor using the wheat cell-free drug screening system

(A) A flow chart of the high-throughput screening to identify the 3-(2,5-dimethyl-1H-pyrrol-1-yl)thiophene-2-carboxylic acid that inhibits the DNA-binding activity of GATA3. The 3-(2,5-dimethyl-1H-pyrrol-1-yl)thiophene -2-carboxylic acid was named pyrrothiogatain (pyrrole and thiofuran containing GATA3 inhibitor). **(B)** The results of the first screen using 9,600 compounds. In the assay, each chemical compound was used at a final concentration of 10 μM. **(C)** The results of the second screening that show the inhibition rate of pyrrothiogatain. The inhibition assay of GATA3 DNA-binding activity was performed in the presence of various concentrations of pyrrothiogatain (0 to 10 μM). Biotinylated FLAG-peptide was used as a control to measure the interference of compounds in the AlphaScreen assay. In addition, a binding assay of RelA and its target DNA was used as control for GATA3. **(D)** Electrophoretic mobility shift assay (EMSA) of GATA3 with its consensus motif containing oligonucleotide in the presence of various concentrations of pyrrothiogatain (0 to 100 μM). GATA3 consensus oligonucleotide labelled with 32P was detected by autoradiography. **(E)** MTS assay to confirm the cytotoxicity of pyrrothiogatain. Jurkat cells were cultured with various concentrations of pyrrothiogatain (0 to 100 μM) for 3 days and subjected to MTS assay. **(F)** HEK293T cells were transfected with firefly luciferase reporter for the Il-5 promoter plus renilla luciferase reporter in the presence (+) or absence (-) of GATA3-expressing plasmid. Then, the cells were left unstimulated (Med.) or stimulated (Stim.) with the phorbol ester PMA (30 ng/mL) in the presence of pyrrothiogatain (0 to 30 μM). The luciferase activity is presented relative to renilla luciferase activity. In (B), (D), and (E), all data are expressed as individual points of three independent experiments with error bars indicating standard deviation.

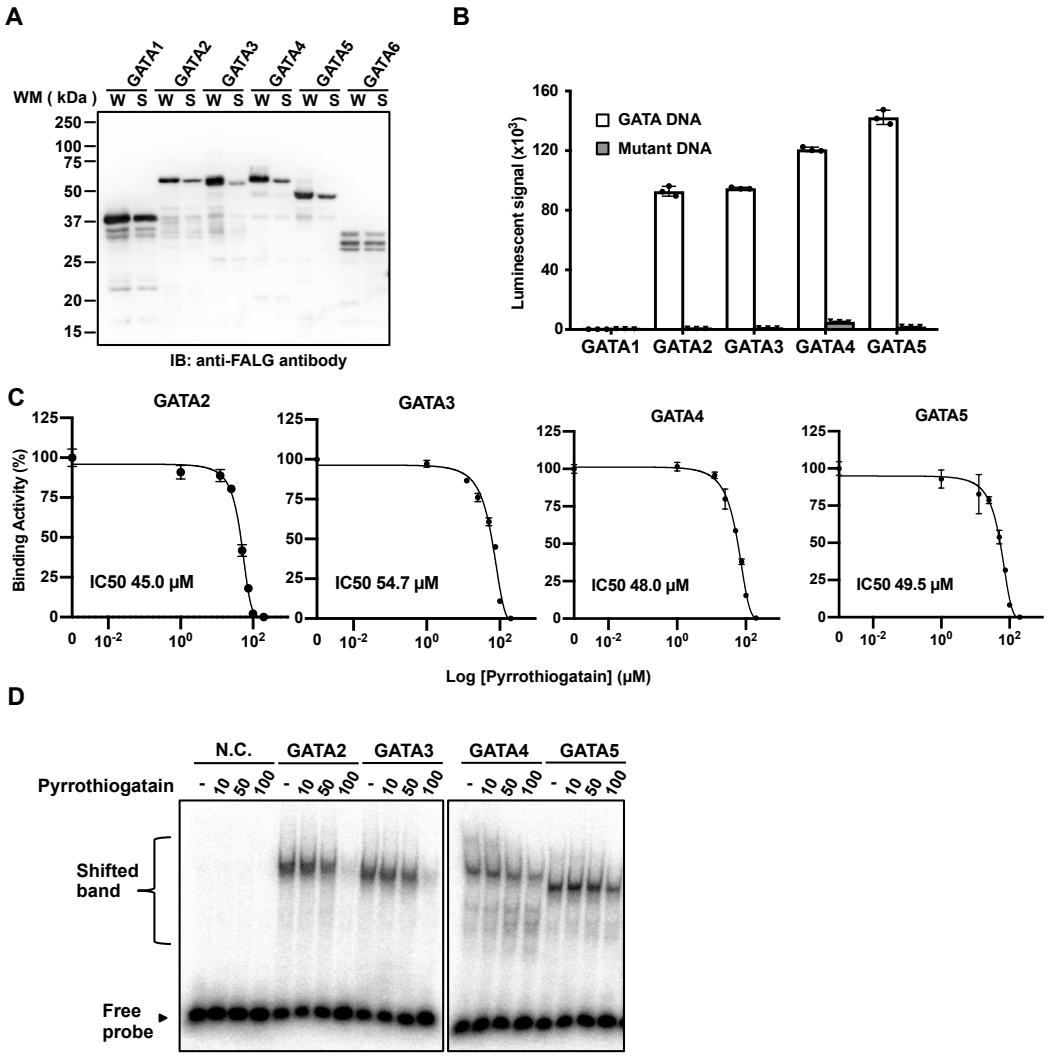

Figure 3 Effect of pyrrothiogatain on the DNA-binding activity of GATA family proteins

(A) Immunoblot analysis of FLAG-tagged recombinant GATA family proteins (GATA1-GATA6) synthesized by the wheat cell-free system. The whole translational mixture (W) and the supernatant (S) were analysed using an anti-FLAG M2 antibody. **(B)** The AlphaScreen assay to detect the binding between the GATA family and DNA containing the GATA consensus binding sequence using the same protocol as that in Figure 1F. **(C)** The inhibition assays for the DNA-binding activity of GATA family proteins (GATA2-GATA5) were performed in the presence of various concentrations of pyrrothiogatain (0 to 200 μM). The binding activity is represented by the relative AlphaScreen signal. **(D)** The results of EMSA of the binding GATA family proteins (GATA2-GATA5) in the presence of pyrrothiogatain (0 to 100 μM). GATA binding to the DNA labelled with 32P was detected by autoradiography. In (B) and (C), all data are expressed as individual points of three independent experiments with error bars indicating standard deviation.

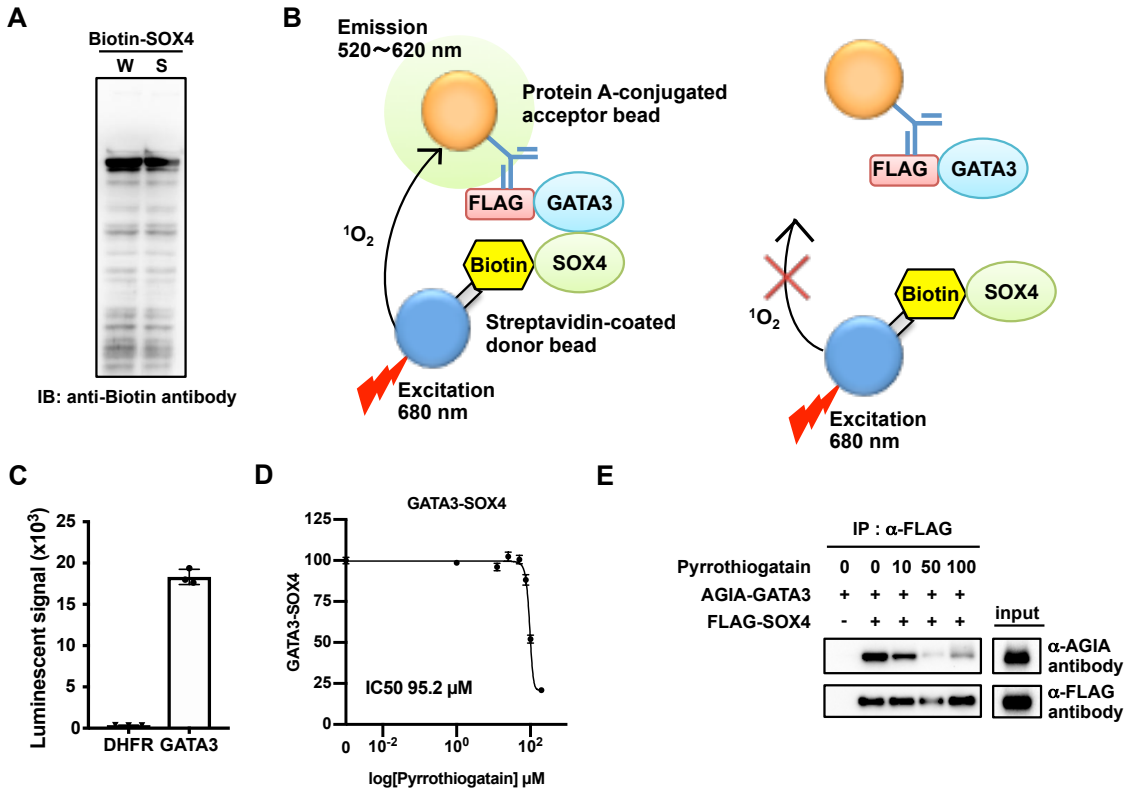

Figure 4 Pyrrothiogatain inhibits the GATA3–SOX4 interaction

(A) Immunoblot analysis of biotin fused recombinant SOX4 (Biotin-SOX4) synthesized by the wheat cell-free system. The whole translational mixture (W) and the supernatant (S) were analysed using an anti-biotin antibody. **(B)** A schematic diagram of the binding assay to detect the direct binding between GATA3 and SOX4. When FLAG-tagged GATA3 binds with biotin fused SOX4, AlphaScreen beads generate a luminescent signal. **(C)** The binding assay of GATA3 and SOX4. The luminescence signals were detected by AlphaScreen technology. FLAG-DHFR was used as a control. **(D)** The inhibition assay of the binding of GATA3 and SOX4 in the presence of various concentrations of pyrrothiogatain (0 to 100 μM). The binding activity was calculated from the AlphaScreen signal. **(E)** The binding of recombinant GATA3 with SOX4 in the presence of pyrrothiogatain (0 to 100 μM) was assessed by immunoprecipitation assay. AGIA-tagged GATA3 and FLAG-tagged SOX4 were synthesized by the wheat cell system and subjected to an immunoprecipitation assay using an anti-FLAG-affinity agarose gel. In (C) and (D), all data are expressed as individual points of three independent experiments with error bars indicating standard deviation.

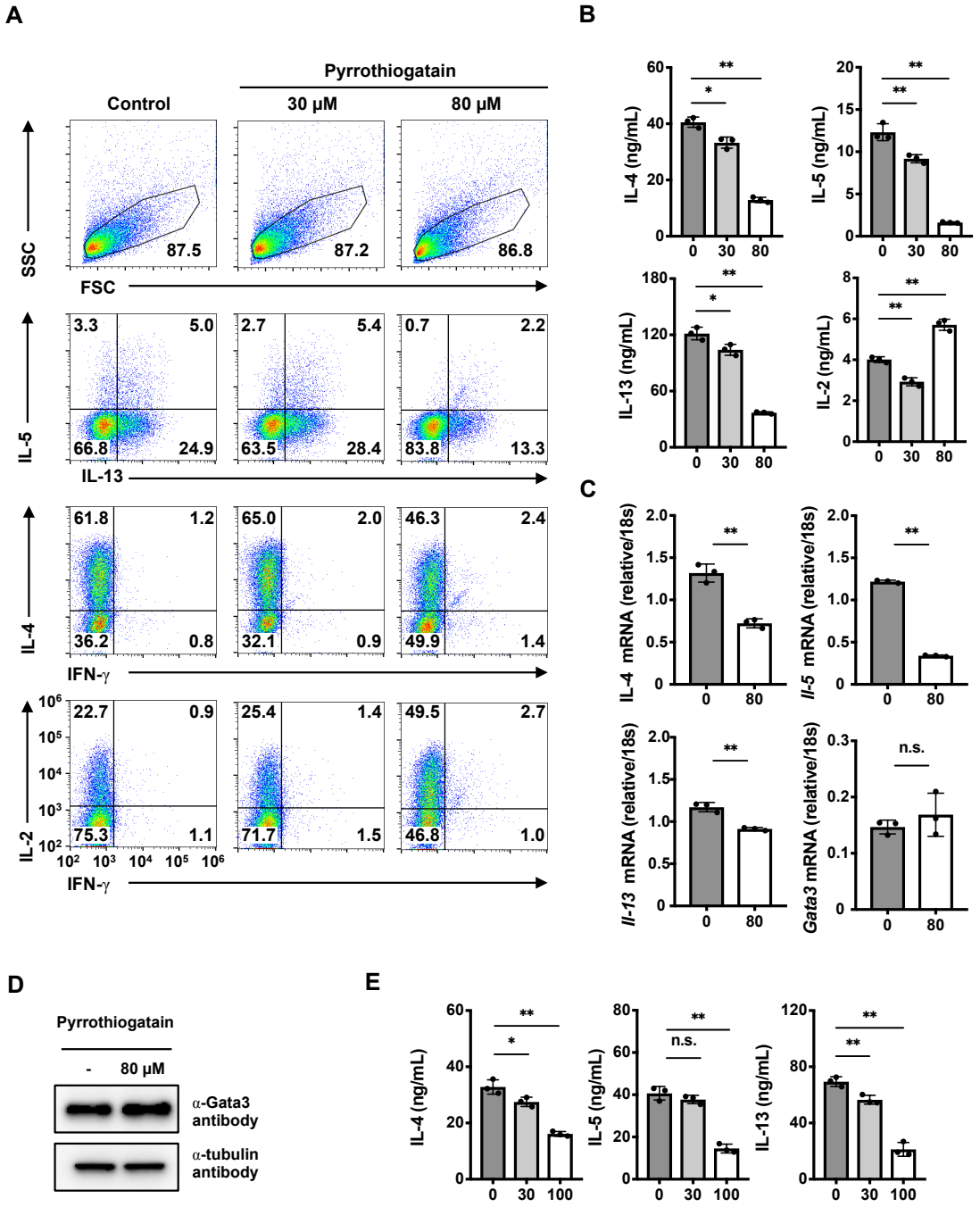

Figure 5 Pyrrothiogatain inhibits Th2 cell differentiation and production of Th2 cytokines

(A) Intracellular staining of IL-5/IL-13, IL-4/IFN-γ, and IL-2/IFN-γ in naive CD4+ T cells cultured under Th2 conditions in the presence or absence of pyrrothiogatain (30 and 80 μM) for five days. **(B)** Cytokine production induced in the pyrrothiogatain treated Th2 cells shown in panel (A) was determined by ELISA. **(C)** Quantitative RT-PCR analysis of the pyrrothiogatain-treated Th2 cells shown in panel (A). **(D)** Immunoblot analysis of GATA3 in naive CD4+ T cells cultured under Th2 conditions in the presence or absence of pyrrothiogatain (80 μM) for 5 days. **(E)** Cytokine production from Th2 cells stimulated with immobilized anti-TCRβ mAb for 16 h in the presence or absence of pyrrothiogatain (0 to 100 μM). The amounts of IL-4, IL-5 and IL-13 in the culture supernatants were determined by ELSA. In (B), (C) and (E), all data are expressed as individual points of three independent experiments with error bars indicating standard deviation.

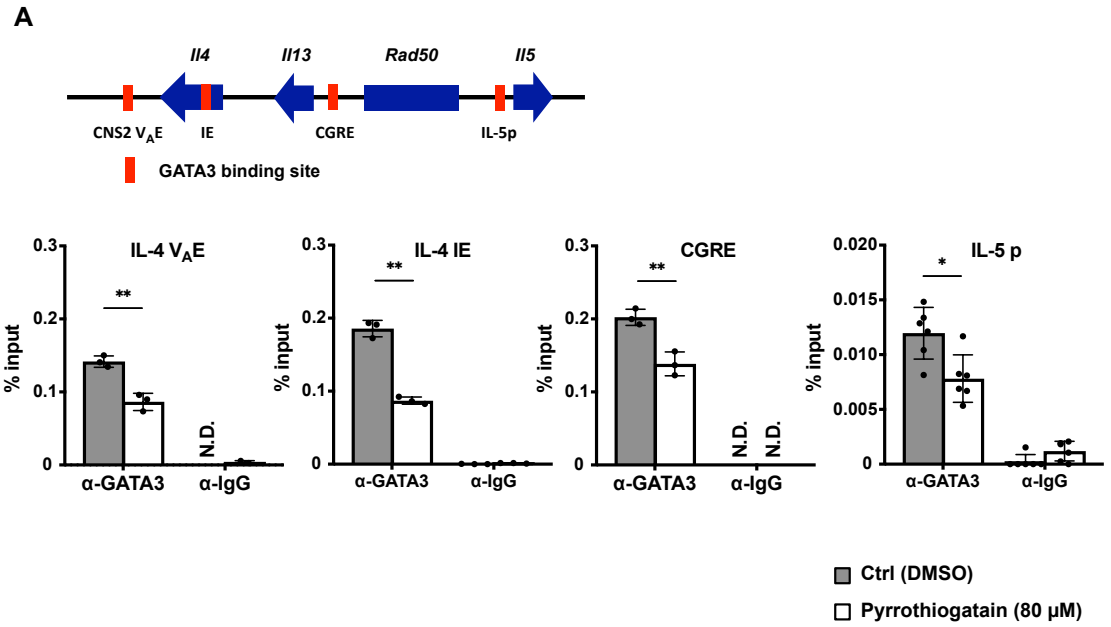

Figure 6 Pyrrothiogatain inhibits GATA3 DNA-binding to Th2 cytokine gene locus

(A) The GATA3 binding sites in Th2 cells are shown as a schematic diagram. Chromatin immunoprecipitation analysis of GATA3 in naive CD4+ T cells cultured under Th2 conditions in the presence or absence of pyrrothiogatain (80 μM) for 2 days. All data are expressed as mean values of three independent experiments with error bars indicating standard deviation.

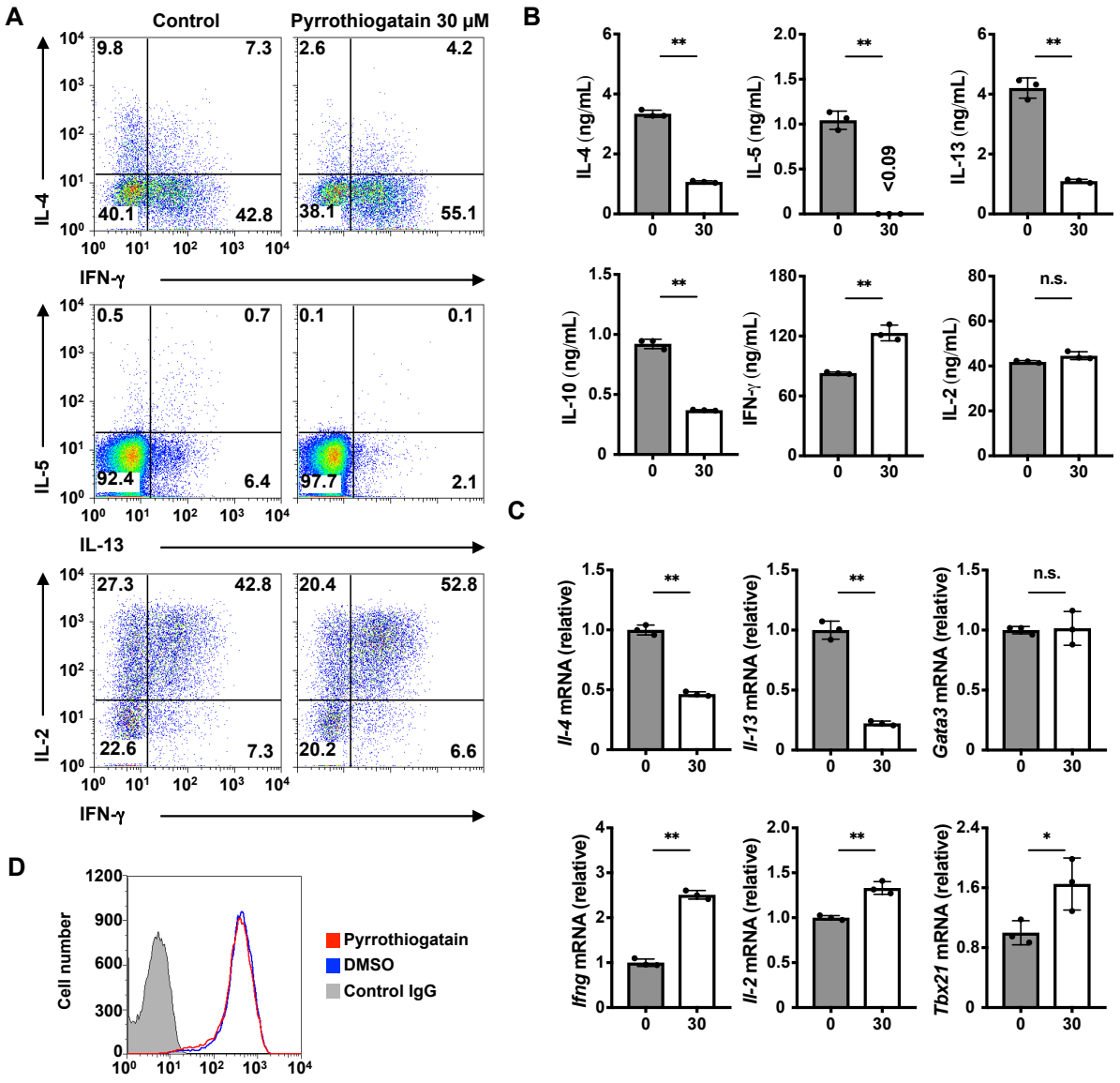

Supplementary Figure S1

(A) Intracellular staining of IL-4/IFN-γ (upper panel), IL-5/IL-13 (middle panel), and IL-2/IFN-γ (lower panel) in CD4+ T cells cultured under IL-2 conditions in the presence or absence of pyrrothiogatain (30 μM) for five days. **(B)** Cytokine production induced in pyrrothiogatain-treated Th2 cells shown in panel (A) was determined by ELISA. **(C)** Quantitative RT-PCR analysis of the pyrrothiogatain-treated Th2 cells shown in panel (A). **(D)** Intracellular staining of GATA3 in CD4+ T cells stimulated with immobilized anti-TCRβ mAb plus anti-CD28 mAb under IL-2 conditions in the presence or absence of pyrrothiogatain (30 μM) for two days.

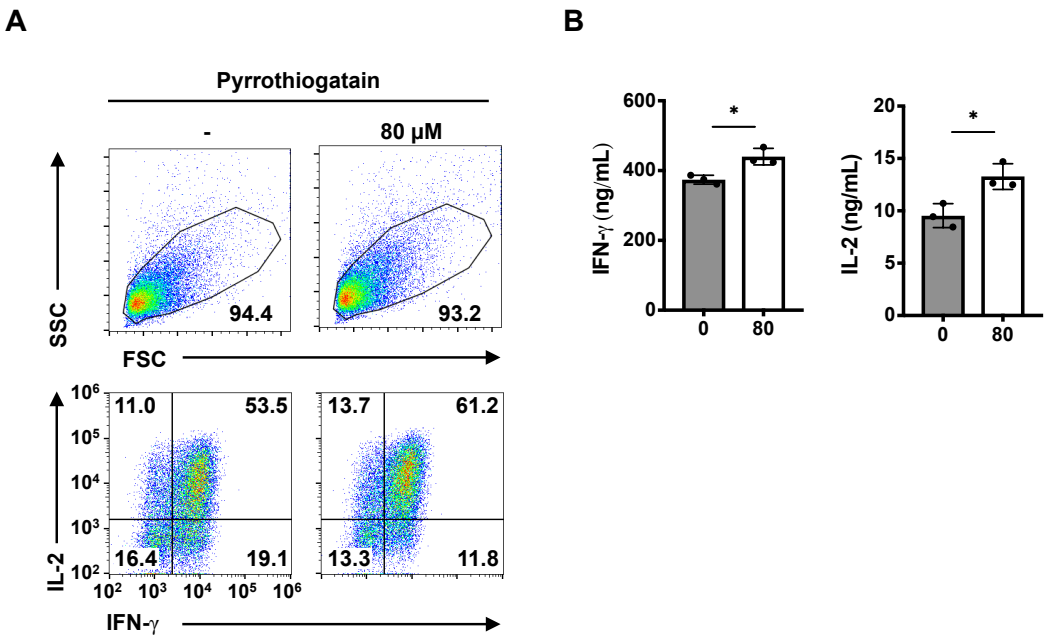

Supplementary Figure S2

(A) Intracellular staining of IL-2/IFN-γ (lower panel) in naive $CD4^+$ T cells cultured under Th1 conditions in the presence or absence of pyrrothiogatain (80 μM) for five days. **(B)** Cytokine production induced in the pyrrothiogatain-treated Th1 cells shown in panel (A) was determined by ELISA.

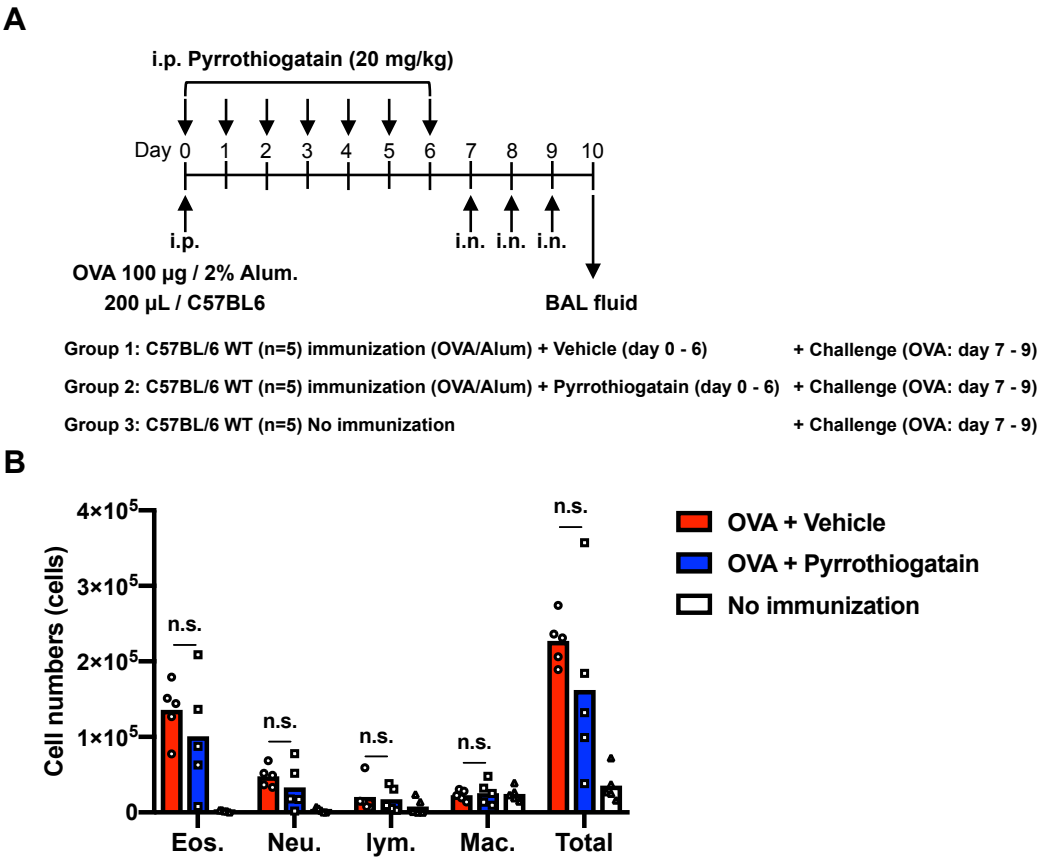

Supplementary Figure S3

(A) A schematic diagram of the experimental protocol of the OVA-induced airway inflammation model. **(B)** The cell count of eosinophils (Eos.), neutrophils (Neu.), lymphocytes (Lym.), macrophages (Mac.), and total cells in BAL Fluid of the model mice shown (n = 5 per group). There was no significant difference between the vehicle control and pyrrothiogatain-administered mice, as detected by ANOVA and Tukey-test.

Chapter II

Glutaminase 1 (Gls1) mediated glutaminolysis regulates Th17 cell dependent immune response

Summary

Glutamine metabolism plays an important role in regulating T cell-dependent immune response, including differentiation of helper T (Th) cell subsets. However, the role of each pathway in the differentiation of $CD4^+$ T cell subsets remains to be elucidated. We herein examined the role of Gls1, which converts glutamine into glutamate by the oxidative deamination, in Th subsets differentiation using T cell-specific *Gls1*-deficient mice.

Gls1 deficiency in $CD4^+$ T cells decreased intracellular glutamate level whereas accumulation of glutamine was observed. Differentiation of Th17 cells was severely impaired in *Gls1*-deficient $CD4^+$ T cells *in vitro.* In contrast, the generation of $Foxp3^+$ iTreg cells was significantly increased in *Gls1*-deficient $CD4^+$ T cells cultured under Th17 conditions.

Gls1-deficeint $CD4^+$ T cells cultured under Th17 conditions decreased glycolysis during early phase of TCR-mediated activation. In contrast, the level of OXPHOS remained unaffected. In vivo, the experimental autoimmune encephalomyelitis was ameliorated in T cell-specific *Gls1*-deficient mice indicating an importance of Gls1 in Th17-dependent immune response.

These results indicate that Th17 cell differentiation is highly dependent on Gls1-mediated glutamine metabolism.

Introduction

Stimulated T cells exit quiescence to induce proliferation and effector differentiation. These processes highly demand the intracellular energy and intermediate metabolite through glycolysis, mitochondrial oxidative phosphorylation (OXPHOS) and Lipid synthesis[1,2]. Activated T cells therefore rely on environmental nutrients, including glucose[3] and amino acids[4-7]. Although inhibition of the nutrients uptakes severely impaired the activation and effector function of T cells[3-6], recent studies indicate that distinct metabolic pathways are used for each Th subsets[8,9]. Therefore, selective modulation of metabolic pathways may permit to ameliorate the inflammation and promote antitumor activity. However, how specific metabolic pathway induces distinct effector T cells remains poorly understood.

Metabolic profiles are distinct among the subtypes of T cells. Whereas naive and memory T cells, similar to non-proliferating cells, rely on OXPHOS and fatty acid oxidation (FAO) for serving intracellular energy[10], aerobic glycolysis characterized for effecter T cells such as Th1, Th2, and Th17 cells promotes T cell activation and differentiation[1,3,10,11]. The glycolysis function is orchestrated by c-Myc[12] and Hif-1α[13] expressing glycolytic enzyme. In particular, HIF-1α robustly promotes anaerobic glycolysis during Th17 cells differentiation and suppressed the induction of iTreg differentiation[13,14].

Glutamine is the most abundant amino acid in the blood and serves as a source of carbon and nitrogen for the synthesis of proteins and biomaterial[15]. Proliferating cells import environmental glutamine and catabolize it into glutamate in both the cytosol and mitochondria. Glutamate further is catabolize into α-ketoglutarate (α-KG), which is supplied into the tricarboxylic acid (TCA) cycle[16]. During glutamine metabolism, glutamine converts into glutamate via two distinct pathways, the amino-group transfer reaction or the oxidative deamination. Although glutamine metabolism plays an important

role in regulating T cell-dependent immune response, including differentiation of Th subets, the role of each pathway in the differentiation of $CD4^+$ T cell subsets remains to be elucidated.

In this study, we herein examined the role of Gls1, which converts glutamine into glutamate via the oxidative deamination in Th cell differentiation using T cell-specific Gls1-deficient mice. *Gls1* deficiency in $CD4^+$ T cells altered the metabolic state decreasing intracellular glutamate level and glycolysis. This change of metabolic state severely impacted for Th17 cell differentiation and Th17 cell dependent immune response. We conclude that Gls1-mediated glutaminolysis regulates Th17 cell differentiation and modulates the Th17/iTreg balance through regulation of metabolic states.

Material and Method

Mice.

Cre TG mice under the control of the *Cd4* promoter were purchased from The Jackson Laboratory. *Gls1* $^{flox/flox}$ and C57BL/6 mice and Clea (Clea Japan, Inc., Tokyo, Japan) respectively. C57BL/6 Gene manipulated mice with C57BL/6 background were used in all experiments. Female mice were used in the *in vivo* experiments. Both male and female mice were used in the *in vitro* experiments. All mice were maintained under specific pathogen-free conditions and used at 6–14 weeks of age. We did not use blind methods. All experiments using mice received approval from Ehime University Administrative Panel for Animal Care. All animal care was conducted in accordance with the guidelines of the Ehime University.

$CD4^+$ T cells stimulation and differentiation *in vitro.*

Naive $CD4^+$ T cells ($CD44l^{ow}CD62L^{high}$) were prepared using a MojoSort^{TM} Mouse CD4 T Cell Isolation Kit (Cat# 480033, BioLegend) and biotin anti-mouse/human CD44 mAb (clone IM7, Cat# 103004, BioLegend) and biotin anti-mouse CD25 mAb (clone PC61, Cat# 102004, BioLegend). Naive $CD4^+$ T cells were stimulates using immobilized anti-TCR-β mAb (10 μg/mL, clone H57-597, BioLegend) plus anti-CD28 mAb (1.0 μg/mL, clone 37.51, Cat# 102116, BioLegend) for 2 days, and then the cells further expanded under similar conditions for an additional 1 day or 3 days. The Th subsets cultured conditions were as follows: IL-2 conditions: IL-2 (10 ng/mL, TONBO Biosciences), Th1 conditions: IL-2 (10 ng/mL, TONBO Biosciences), IL-12 (1 ng/mL, Pepro Tech), and anti-IL-4 mAb (2.5 μg/mL, clone 11B11, BioLegend). Th2 conditions: IL-2 (10 ng/mL, TONBO Biosciences), IL-4 (3 ng/mL, Pepro Tech), and anti-IFN-γ mAb (2.5 μg/mL, clone XMG1.2, BioLegend). Th17 conditions (TGF-β condition): IL-6 (10 ng/mL, Fujifilm

Wako), IL-1β (10 ng/mL, Fujifilm Wako), TGF-β (1 ng/mL, R&D system), anti-IFN-γ mAb (2.5 μg/mL, clone XMG1.2, BioLegend), anti-IL-4 mAb (2.5 μg/mL, clone 11B11, BioLegend), anti-IL-2 (2.5 μg/mL, clone JES6-1A12, BioLegend), Th17 conditions (IL-23 condition): IL-6 (20 ng/mL, Fujifilm Wako), IL-1β (10 ng/mL, Fujifilm Wako), IL-23 (10 ng/mL, R&D system), anti-IFN-γ mAb (2.5 μg/mL, clone XMG1.2, BioLegend), anti-IL-4 mAb (2.5 μg/mL, clone 11B11, BioLegend), anti-IL-2 (2.5 μg/mL, clone JES6-1A12, BioLegend), Th9 conditions: IL-2 (10 ng/mL, TONBO Biosciences), IL-4 (3 ng/mL, Pepro Tech), TGF-β (3 ng/mL, R&D system) and anti-IFN-γ mAb (2.5 μg/mL, clone XMG1.2, BioLegend). iTreg conditions: IL-2 (10 ng/mL, TONBO Biosciences), TGF-β (1 ng/mL, R&D system), anti-IFN-γ mAb (2.5 μg/mL, clone XMG1.2, BioLegend) and anti-IL-4 mAb (2.5 μg/mL, clone 11B11, BioLegend). The cultured cells were subjected to further analysis.

Intracellular staining of cytokines and transcription factors and surface staining

The *in vitro* differentiated $CD4^+$ T cells were stimulated using an immobilized anti-TCR-β mAb (10 μg/ml, clone H57–597, BioLegend) for 6 h in the presence of monensin (2 μM). After stimulation, the cells were fixed with 4% paraformaldehyde (Cat# 163–20145, Fujifilm Wako) and permeabilized with permeabilization buffer (50 mM NaCl, 5 mM EDTA, 0.02% NaN3, and 0.5% Triton X-100). Then, the cells were stained using antibodies in the Table. For the intracellular staining of transcription factor, the Foxp3/Transcription Factor Staining Buffer Kit (Cat# TNB-0607, TONBO Biosciences) was used according to the manufacturer's protocol. For surface staining, collected cells were washed with PBS followed by staining with antibodies in the Table. Flow cytometry was performed using a Gallios Flow Cytometer instrument (Beckman Coulter) and the results were analyzed using the FlowJo software program (Tree Star, Ashland, OR, USA).

ELISA assay

The *in vitro* differentiated $CD4^+$ T cells were stimulated using an immobilized anti-TCR-β mAb (10 μg/ml, clone H57–597, BioLegend) for 16 h, and the culture supernatants were recovered. The amounts of the cytokines in the recovered supernatant were determined using the reagent and antibodies in the Table.

QRT-PCR

Total mRNA of the *in vitro* differentiated $CD4^+$ T cells was purified with TRI Reagent (Cat# TR118, Molecular Research Center). cDNA was synthesized using the SuperScript™ VILO™ Master Mix (Cat# 11755050, Thermo Fisher scientific). The reaction of qRT-PCR was performed with Step One Plus Real-Time PCR System (Thermo Fisher scientifics). The reagent and primers for qRT-PCR reaction were described in the Table.

Immunoblot analysis

The cytoplasmic and nuclear lysates of *in vitro* differentiated $CD4^+$ T cells were recovered using NE-PER™ Nuclear and Cytoplasmic Extraction Reagents (Cat# 78833, Thermo scientifics), according to the manufacture's protocol. The lysates were separated by SDS-PAGE and blotted onto PVDF membrane (GE Healthcare). The blotted proteins were detected with the specific antibody described in the Table.

Experimental Autoimmune Encephalomyelitis

Mice (8–12 weeks old) were immunized by subcutaneous injection with an emulsion containing the myelin oligodendrocyte glycoprotein (MOG) peptide $MOG_{35–55}$ (100 μg/mouse, Quality Controlled Biochemicals, >95% purity, BEX Co., Ltd) and M.

tuberculosis H37Ra extract (5 mg/mL Cat# 231141, BD Difco Laboratories) in CFA. In addition, pertussis toxin (50 ng/mouse, Cat# 180, List Biological Laboratories) was administrated intraperitoneally on days 0 and 2. Mice were weighed and monitored for determining clinical score according to the following signature: 0, healthy; 0.5, partially limp tail; 1, complete limp tail; 2, gait ataxia; 3, partial hind limb paralysis; 4, hind limb paralysis; 5, fore limb and hind limb paralysis; 6, moribundity or death.

Analysis of $CD4^+$ T cells infiltrating to spinal cord in EAE-induced mice

Spinal cords of EAE-induced mice at peak of clinical score were extruded from spinal canal with PBS by hydraulic pressure. The spinal cords were chopped up and digested using collagenase D (2.5 mg/mL Cat# 11088858001, Roche) and DNase I (1 mg/mL, Cat# 10104159001, Roche) at 37ºC for 20 min. The tissues were passed through 70 mm cell strainer, followed a 35.7% parcol centrifugation. The isolated cells were recovered from precipitate and stimulated with PMA (10 ng/mL) and Ionomycin (1 μM) in the presence of monesin (2 μM) for 4 h, followed by intracellular staining.

Histological analysis of spinal cord in EAE-induced mice

Spinal cords of EAE-induced mice at peak of clinical score were extruded from spinal canal with PBS by hydraulic pressure and then fixed with 4% paraformaldehyde (Cat# 163–20145, Fujifilm Wako) at 4ºC for over night. The spinal cords were embedded by paraffin and stained with H&E or Luxol fast blue stains.

Metabolic analysis

Metabolites measurements and data processing were performed through a facility service at Human Metabolome Technology Inc. (Yamagata, Japan). Briefly, naive $CD4^+$ T cells were

stimulated with immobilized anti-TCR-β mAb (10 μg/mL, clone H57-597, BioLegend) plus anti-CD28 mAb (1.0 μg/mL, clone 37.51, Cat# 102116, BioLegend) for 24 h.

The cultured $CD4^+$ T cells (5 x 10^6 cells) were washed twice with 10 mL of 5% (w/w) mannitol and then lysed with and then lysed with 1 ml of methanol containing internal standards, 25 μM L-Methionine sulfone (Cat# 502-76641, Wako) and 2-Morpholinoethanesulfonic acid, monohydrate (Cat# 349-01623, Doujindo) and D-Camphor-10-sulfonic Acid Sodium Salt (Cat# 037-01032, Wako). 400 μL of chloroform and 200 μL of Milli-Q water were added to 400 μL of the extracted and mixed well. After centrifuged at 10,000× g at 4 °C for 3 min, 400 μL of the upper aqueous layer was centrifugally filtered through a Millipore 5-kDa cutoff filter (Cat# UFC30VV25, Millipore) at 9100 × g at 4 °C for 120 min to remove proteins. The filtrate was centrifugally concentrated and resuspended in 25 μl of Milli-Q water containing internal standards 200 μM 3-Aminopyrrolidine (Cat# 404624, Sigma Aldrich) and 1,3,5-Benzenetricarboxylic Acid (Cat# 206-03641, Wako) for the capillary electrophoresis mass spectrometry (CE-MS). Cationic compounds were measured in the positive mode of capillary electrophoresis-time of flight-mass spectrometry (CE-TOFMS) and anionic compounds were measured in the positive and negative modes of capillary electrophoresis-tandem mass spectrometry (CE-MS/MS) in accordance with the methods developed by Soga et al.

In some experiments, the intracellular glutamate concentration was determined using a Glutamate Colorimetric Assay Kit (cat# K629-100, BioVision) according to the manufacture's protocol.

The extracellular acidification rate (ECAR) and oxygen consumption rate (OCR) were measured using an Extracellular Flux Analyzer XFp (Agilent Technologies). The culture medium was changed to Seahorse XF RPMI Base Medium (Cat#103336-100) before the analysis. Activated $CD4^+$ T cells (1 × 10^5 cells) were adhered on Cell Tak coated seahorse

8-well plate and were pre-incubated at 37 °C for 60 min in the absence of CO_2. The ECAR were measured at the baseline and in response to 10 mM glucose, 1 μM oligomycin and 50 mM 2-DG (XFp glycolysis stress test kit; cat#103017-100; Agilent Technologies). The OCR was measured under basal conditions and in response to 1 μM oligomycin, 2 μM FCCP, and 0.5 μM rotenone/antimycin A (XFp mito stress test kit; cat#103010-100; Agilent Technologies).

Statistical analysis and number of replicates per experiments

Statistical significance was calculated using two-tailed unpaired Student's t-test (Microsoft Excel and Graphpad prism 8). Statistical significance was accepted at $p < 0.05$.

Results

Gls1 deficiency alters the intracellular metabolic status by TCR stimulation.

In order to investing the intrinsic roles of Gls1 in T cell functions, T cell specific *Gls1*-deficient mice were generated by crossing *Gls1*$^{flox/flox}$ mice with *CD4-Cre* transgenic (TG) mice. *Gls1*-dificiency did not affect the development and homeostasis of T cell in thymus and spleen (Supplementary Fig. 1A and 1B). In addition, the development of thymus-derived natural Treg (nTreg) in *Gls1*-dificiency mice was comparable with WT mice (Supplementary Fig. 1C). The resting T cells with normal phenotype in *Gls1*-dificienent mice permits us to investigate how Gls1-mediated metabolic change impact for T cell functions and fates.

Stimulated T cells uptake glucose and amino acids to induce metabolic reprograming through glycolysis and glutaminolysis (Fig. 1A)[6,12]. The metabolites produced by the catabolic reaction are accumulated at 24 hr before entering into the cell cycle and used for anabolic pathways[12]. To investigate how *Gls1* deficiency alters the intracellular metabolic status by TCR-mediated activation, naive CD4$^+$ T cells stimulated with α-TCR-β mAb plus α-CD28 mAb for 24 h were subjected to the metabolic analysis with capillary electrophoresis mass spectrometry (CE-MS). As expected, *Gls1*-deficiency led to amount of intracellular glutamate decreased whereas accumulation of glutamine is observed (Fig. 1B). In addition, the amino acids, such as aspartate and branched-chain amino acids, used for producing glutamate were decreased in *Gls1* KO CD4$^+$ T cells (Supplementary Fig. 2). TCA intermediates, produced with glutaminolysis, such as succinate, fumarate and malate were decreased in *Gls1* KO CD4$^+$ T cells (Fig. 1C). Although intracellular lactate level of an end-product of anaerobic glycolysis is not altered, other glycolytic metabolites such as glucose 6-phosphate and fructose 1,6-diphosphate was significantly decreased in *Gls1* KO

$CD4^+$ T cells (Fig. 1D). These results indicate that *Gls1*-deficiency decreased the intracellular level of TCA and glycolytic intermediated metabolites as well as glutamate.

Differentiation of Th17 is selectively impaired in *Gls1*-difficient $CD4^+$ T cells

Distinct cytokine lead to alter the metabolic state as well as the fate of Th subsets differentiation[17]. However, the expression level of Gls1 is no difference among $CD4^+$ T cells cultured under each Th subsets conditions (Supplementary Fig. 3). Next, we assessed the effect of Gls1 deficiency on Th subsets differentiation. The generation of IL-17A- and IL-17F-producing cells was decreased in *Gls1*-difficient $CD4^+$ T cells cultured under both Th17 and pathogenic Th17 conditions compared with WT (Fig. 2A and Supplementary Fig. 4A). The decreased production of IL-17A and IL-17F was confirmed using ELISA (Fig. 2B). Similarly, the treatment of Gls1 inhibitor CB-839 repressed the differentiation of Th17 cells and the Th17 cytokines production (Supplementary Fig. 4A and 4B). However, the inductions of IFN-γ- and IL-2-producing Th1 cells, Foxp3-positive iTreg and IL-9-producing Th9 were not much affected with *Gls1* deficiency (Supplementary Fig. 5B-5E), whereas the generation of IL-5 and IL-13 producing Th2 cells was increased in *Gls1* deficient $CD4^+$ T cells (Supplementary Fig. 5H and 5I). However, the analysis OVA-induced allergy airway inflammation model showed that the increase of Th2 dependent response was not admitted in *Gls1*-deficient mice (Supplementary Fig. 6).

In order to examine the expression level of characteristic genes in Th17 cells, the expression levels of IL-22 and IL-23r mRNA was decreased in *Gls1*-deficient Th17 cells compared with WT Th17 cells (Fig. 2C). Interestingly, the expression level of Rorα regulating IL-17A and IL-17F and Rorγt identified as master regulator of Th17 cells were not much influenced in *Gls1*-deficient Th17 cells (Fig. 2D-2F). These results indicate that Gls1-mediated metabolic pathway is important for Th17 cell differentiation.

Th17 cell dependent inflammation is ameliorated in T cell-specific *Gls1*-deficient mice

Our *in vitro* results showed that the both genetic inactivation and pharmaceutical inhibition of the Gls1 function repressed the Th17 cell differentiation. In order to investigate the intrinsic role of Gls1 for the Th17 cell dependent inflammation *in vivo*, we induced the Experimental Autoimmune Encephalomyelitis (EAE) in mice. As shown Fig 3A weight reduction and clinical symptom of EAE were more modulated in *Gls1*-deficient mice than WT mice. Similarly, CB-839 administration delayed the onset of EAE compared with vehicle control (Supplementary Fig. 6). Correlated with clinical symptom, infiltration of inflammatory cells into central nervous system (CNS) and demyelination of spinal cord in *Gls1*-deficient mice were repressed compared with WT mice (Fig. 3B). Furthermore, IL-17A and IFN-γ producing $CD4^+$ T cells in *Gls1*-deficient mice less infiltrate central nervous system (CNS) than in WT mice (Fig. 3C and 3D). Theses results indicate that Gls1-mediated glutaminolysis is important for Th17 cell dependent inflammation.

***Gls1*-deficiency suppresses glycolytic activity of Hif-1α and alters Th17/Treg balance.**

To confirm that *Gls1*-deficiency reduces the level of intracellular glutamate during Th17 cell differentiation, the level of intracellular glutamate were determined in *Gls1*-deficient naive $CD4^+$ T cells cultured under Th17 conditions for 24 h. The intracellular glutamate concentration was decreased in *Gls1*-deficient naive $CD4^+$ T cells cultured under Th17 conditions compared with WT (Fig. 4A). Intracellular glutamate is converted into α-KG to replenish TCA cycle intermediate. We therefore assessed whether or not the supplementation of α-KG rescues *Gls1*-dificient phonotype. However, the suppressions of Th17 cell differentiation and Th17 cytokine production by *Gls1*-decifiency were not rescued with supplementation of DM-α-KG (Fig. 4B and 4C).

To investigate how *Gls1*-deficiency impact the metabolic state for Th17 cell differentiation, naive $CD4^+$ T cells cultured under Th17 conditions for 24 h were subjected to the metabolic analysis. Furthermore, glycolysis was drastically decreased in *Gls1*-deficeint $CD4^+$ T cells cultured under Th17 conditions whereas the level of OXPHOS remained unaffected (Fig. 4D). During T cell differentiation, glycolysis is induced by c-Myc[12] and Hif-1α[13,14]. In particular, HIF-1α robustly promotes glycolysis during Th17 cells differentiation and suppressed the induction of iTreg differentiation[13,14]. We therefore examined the expression level of c-Myc and Hif-1α in *Gls1*-deficient $CD4^+$ T cells during Th17 cell differentiation. The expressions of c-Myc and Hif-1α were not affected at mRNA level in *Gls1*-deficient naive $CD4^+$ T cells (Fig. 4E). However, the expressions of c-Myc and Hif-1α were decreased in *Gls1*-deficient naive $CD4^+$ T cells at protein level (Fig. 4F). In addition, the expressions of glucose transporter such as slc2a1 and slc2a3 were mildly decreased in *Gls1*-deficient naive $CD4^+$ T cells (Fig. 4G). In order to assess whether or not the decreased Hif-1α in *Gls1*-deficient Th17 cells induce the differentiation of iTreg, *Gls1*-deficient naive $CD4^+$ T cells were cultured under Th17 conditions in the presence or absence of α-IL-2 neutralizing mAb. Interestingly, the generation of Foxp3-positive iTreg was increased in *Gls1*-deficient $CD4^+$ T cells under Th17 conditions without α-IL-2 (Fig. 4H). Although *Gls1*-deficiency promoted the generation of iTreg during Th17 cell differentiation, the expression level of phospho-Sata3 and Stat5 in nucleus was not influence with *Gls1*-deficifency (Supplementary Fig. 8).

Several reports indicates that reactive oxygen species (ROS) is essential for T cell effector function[18,19] whereas the excessive ROS production inhibits the enzyme of glycolysis[20] and Th17 cell differentiation[8,21]. Conventionally, the excessive ROS is buffered by reduced glutathione (GSH) synthesized from cysteine, glycine and glutamate. To examine that whether or not the dysregulation of ROS cause Th17 cell differentiation,

Gls1-deficient naive $CD4^+$ T cells cultured under Th17 conditions were subjected to the analysis of the intracellular redox state. Compared with WT, the level of intracellular ROS is not influenced in *Gls1*-deficient Th17 cells (Supplementary Fig. 9A). Similarly, Gls1-deficiency did not affect the levels of intracellular GSH and total glutathione (Supplementary Fig. 9B and 9C). In addition, supplementation of the glutathione mimic N-acetyl cysteine (NAC) did not rescue the suppression of Th17 differentiation in *Gls1*-deficient $CD4^+$ T cells (Supplementary Fig. 9D).

Theses results indicated that *Gls1*-deficiency suppressed glycolytic activity of Hif-1α and alters Th17/Treg balance through changing metabolic state.

Discussion

Previous reports indicated that glutamine is essential for T cell activation and the differentiation of Th subsets[4,6,22]. In addition, glutamine-dependent α-KG production is necessary for Th1 cell differentiation[17,22]. Gls1 works as the first enzyme of glutaminolysis and contributes the production of α-KG[16]. Our results however indicated that *Gls1*-deficiency repressed only the Th17 cell differentiation (Figure 1 and Supplementary Fig. 5) despite Gls1 was highly expressed in all Th subsets (Supplementary Fig. 3). In addition, α-KG supplementation did not rescue the impairment of Th17 cell differentiation in *Gls1*-deficient $CD4^+$ T cells (Figrue 4B and 4C), implying the impairment of Th17 cell differentiation by *Gls1* deficiency is not due to the decrease of α-KG. In addition, α-KG regulates metabolic change cooperating IL-2 signaling sensitively[17]. Although α-KG supports the induction of Th17 cell through the production of 2-hydroxyglutarat (2-HG)[9], the requirement of α-KG for Th17 cells may be less than other Th subsets induced by IL-2.

Although *Gls1*-deficinecy severely reduced the levels of intracellular glutamate (Fig. 1B and Fig. 4A), glutamate must be supplied through other pathways for the synthesis of protein and glutathione. In cancer research, branched-chain-amino-acid aminotransferase (Bcats) catabolizing Leu, Ile and Val into glutamate, works complementary roles of Gls1 in glutamate and glutathione biosynthesis[23]. Also, Bcats may support the glutamate biosynthesis in *Gls1*-deficiency $CD4^+$ T cells because the amounts of intracellular branched-chain amino acids such as valine, leucine and isoleucine were decreased in *Gls1* deficient $CD4^+$ T cells (Supplementary Fig. 2). In addition, another reports indicated that Bcats repressed the glycolysis through mTORC1 signaling in $CD4^+$ T cells[24].

Gls1-deficiency repressed Th17 cell differentiation but induced the generation of $Foxp3^+$ iTreg during Th17 cell conditions (Figure 4H). Whereas Th17 cell differentiation rely on glycolysis, OXPHOS and Lipid synthesis, the induction of iTreg do not much demand

glycolysis[25,26]. In addition, the ablation of Hif-1α inducing glycolytic enzyme repressed Th17 cell differentiation and promotes the induction of iTreg[13,14]. These reports support that suppression of glycolytic activity and Hif-1α expression by *Gls1*-deficiency altered the balance of Th17/iTreg. Also, IL-2/STAT5 signaling induced iTreg differentiation but repressed Th17 cell differentiation through inhibition of STAT3 function[27-29]. However, the expression level of p-STAT3 and p-STAT5 in nucleus was not influenced (Supplementary Figure 8). Therefore, Gls1-dependent metabolic regulation supports glycolysis through Hif-1α and controls the balance of Th17/iTreg.

In conclusion, these results indicated that the important glutamine metabolic pathway is distinct for differentiation of Th subsets. *Gls1* deficiency in $CD4^+$ T cells altered the metabolic state decreasing intracellular glutamate level and glycolysis. This change of metabolic state by *Gls1* deficiency severely impacted for Th17 cell differentiation and inducing iTreg cell differentiation. Therefore, Gls1 is attractive drug target for suppressing Th17 dependent inflammation and inducing immune tolerance through promoting of iTreg differentiation.

Reference

1. Wang, R. & Green, D. R. Metabolic checkpoints in activated T cells. *Nature Immunology* **13,** 907–915 (2012).
2. Chapman, N. M., Boothby, M. R. & Chi, H. Metabolic coordination of T cell quiescence and activation. *Nature Publishing Group* **12,** 478–70 (2019).
3. Macintyre, A. N. *et al.* The glucose transporter Glut1 is selectively essential for CD4 T cell activation and effector function. *Cell Metabolism* **20,** 61–72 (2014).
4. Nakaya, M. *et al.* Inflammatory T cell responses rely on amino acid transporter ASCT2 facilitation of glutamine uptake and mTORC1 kinase activation. *Immunity* **40,** 692–705 (2014).
5. Sinclair, L. V. *et al.* Control of amino-acid transport by antigen receptors coordinates the metabolic reprogramming essential for T cell differentiation. *Nature Immunology* **14,** 500–508 (2013).
6. Carr, E. L. *et al.* Glutamine uptake and metabolism are coordinately regulated by ERK/MAPK during T lymphocyte activation. *J. Immunol.* **185,** 1037–1044 (2010).
7. Ron-Harel, N. *et al.* T Cell Activation Depends on Extracellular Alanine. *Cell Rep* **28,** 3011–3021.e4 (2019).
8. Gerriets, V. A. *et al.* Metabolic programming and PDHK1 control CD4+ T cell subsets and inflammation. *J. Clin. Invest.* **125,** 194–207 (2015).
9. Xu, T. *et al.* Metabolic control of TH17 and induced Treg cell balance by an epigenetic mechanism. *Nature* **548,** 228–233 (2017).
10. Geltink, R. I. K., Kyle, R. L. & Pearce, E. L. Unraveling the Complex Interplay Between T Cell Metabolism and Function. *Annu. Rev. Immunol.* **36,** 461–488 (2018).
11. Chang, C.-H. *et al.* Posttranscriptional control of T cell effector function by aerobic glycolysis. *Cell* **153,** 1239–1251 (2013).
12. Wang, R. *et al.* The transcription factor Myc controls metabolic reprogramming upon T lymphocyte activation. *Immunity* **35,** 871–882 (2011).
13. Shi, L. Z. *et al.* HIF1alpha-dependent glycolytic pathway orchestrates a metabolic checkpoint for the differentiation of TH17 and Treg cells. *J. Exp. Med.* **208,** 1367–1376 (2011).
14. Dang, E. V. *et al.* Control of T(H)17/T(reg) balance by hypoxia-inducible factor 1. *Cell* **146,** 772–784 (2011).
15. DeBerardinis, R. J. & Cheng, T. Q's next: the diverse functions of glutamine in metabolism, cell biology and cancer. *Oncogene* **29,** 313–324 (2010).
16. Jin, L., Alesi, G. N. & Kang, S. Glutaminolysis as a target for cancer therapy. *Oncogene* **35,** 3619–3625 (2016).

17. Chisolm, D. A. *et al.* CCCTC-Binding Factor Translates Interleukin 2- and α-Ketoglutarate-Sensitive Metabolic Changes in T Cells into Context-Dependent Gene Programs. *Immunity* **47,** 251–267.e7 (2017).
18. Mak, T. W. *et al.* Glutathione Primes T Cell Metabolism for Inflammation. *Immunity* **46,** 675–689 (2017).
19. Sena, L. A. *et al.* Mitochondria are required for antigen-specific T cell activation through reactive oxygen species signaling. *Immunity* **38,** 225–236 (2013).
20. Nakao, K., Minato, N., Uemoto, S., Mullarky, E. & Cantley, L. C. Diverting Glycolysis to Combat Oxidative Stress. (2015). doi:10.1007/978-4-431-55651-0_1
21. Johnson, M. O. *et al.* Distinct Regulation of Th17 and Th1 Cell Differentiation by Glutaminase-Dependent Metabolism. *Cell* **175,** 1780–1795.e19 (2018).
22. Klysz, D. *et al.* Glutamine-dependent α-ketoglutarate production regulates the balance between T helper 1 cell and regulatory T cell generation. *Sci Signal* **8,** ra97–ra97 (2015).
23. McBrayer, S. K. *et al.* Transaminase Inhibition by 2-Hydroxyglutarate Impairs Glutamate Biosynthesis and Redox Homeostasis in Glioma. *Cell* **175,** 101–116.e25 (2018).
24. Ananieva, E. A., Patel, C. H., Drake, C. H., Powell, J. D. & Hutson, S. M. Cytosolic branched chain aminotransferase (BCATc) regulates mTORC1 signaling and glycolytic metabolism in CD4+ T cells. *J. Biol. Chem.* **289,** 18793–18804 (2014).
25. Angelin, A. *et al.* Foxp3 Reprograms T Cell Metabolism to Function in Low-Glucose, High-Lactate Environments. *Cell Metabolism* **25,** 1282–1293.e7 (2017).
26. Michalek, R. D. *et al.* Cutting edge: distinct glycolytic and lipid oxidative metabolic programs are essential for effector and regulatory CD4+ T cell subsets. *J. Immunol.* **186,** 3299–3303 (2011).
27. Laurence, A. *et al.* Interleukin-2 signaling via STAT5 constrains T helper 17 cell generation. *Immunity* **26,** 371–381 (2007).
28. Durant, L. *et al.* Diverse targets of the transcription factor STAT3 contribute to T cell pathogenicity and homeostasis. *Immunity* **32,** 605–615 (2010).
29. Yang, X.-P. *et al.* Opposing regulation of the locus encoding IL-17 through direct, reciprocal actions of STAT3 and STAT5. *Nature Immunology* **12,** 247–254 (2011).

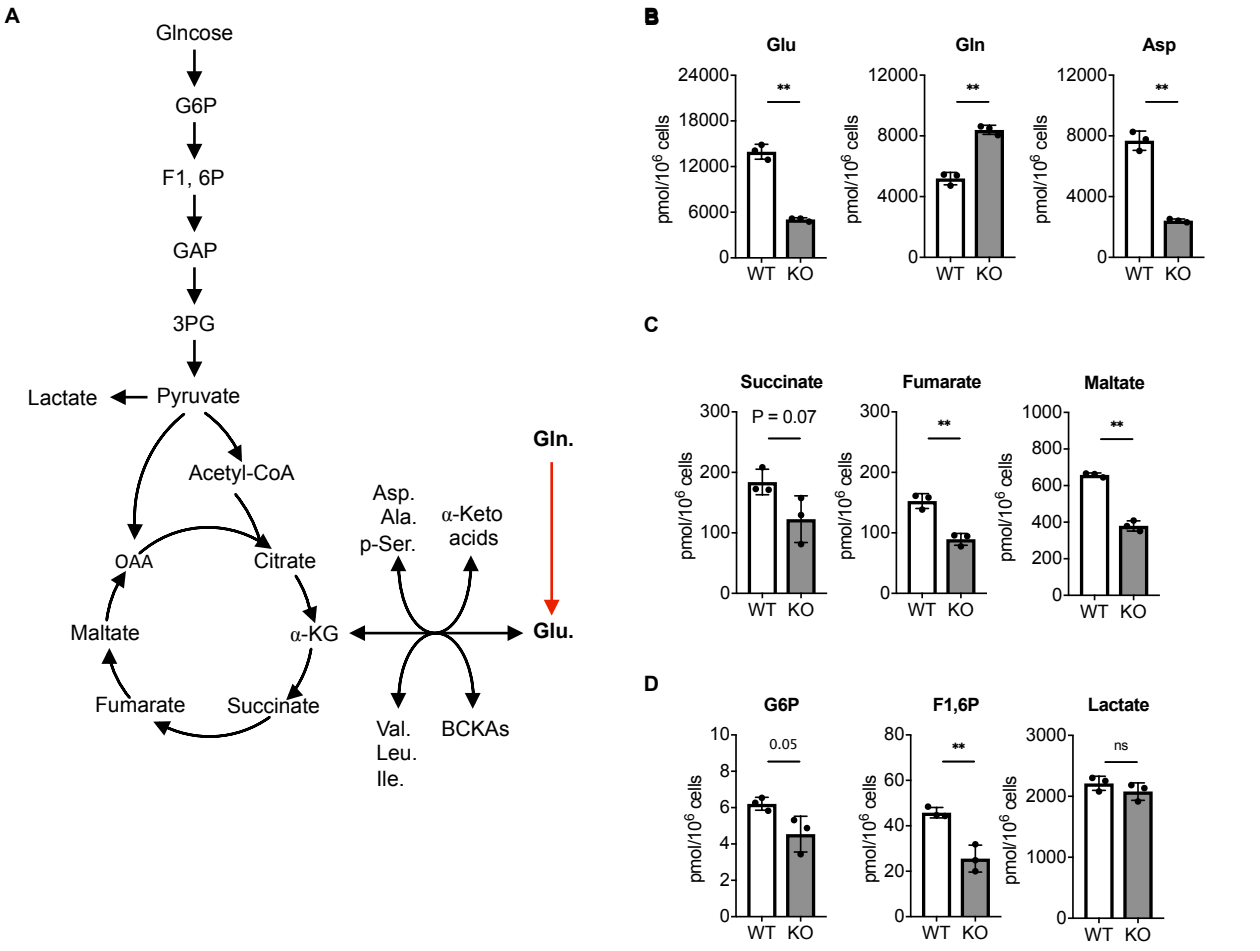

Figure 1 *Gls1* deficiency alters the intracellular metabolic status by TCR stimulation.

(A) Schematic diagram of glycolysis and glutaminolysis. **(B)** The Intracellular level of amino acids in WT or Gls1 KO naive $CD4^+$ T cells stimulated with immobilized α-TCR-β mAb plus α-CD28 mAb for 24 h. **(C)** The Intracellular level of TCA intermediate metabolites in cells of (B). **(D)** The Intracellular level of glycolytic metabolites in cells of (B). In (B), (C) and (D), all data are expressed as individual points of three independent experiments with error bars indicating standard deviation.

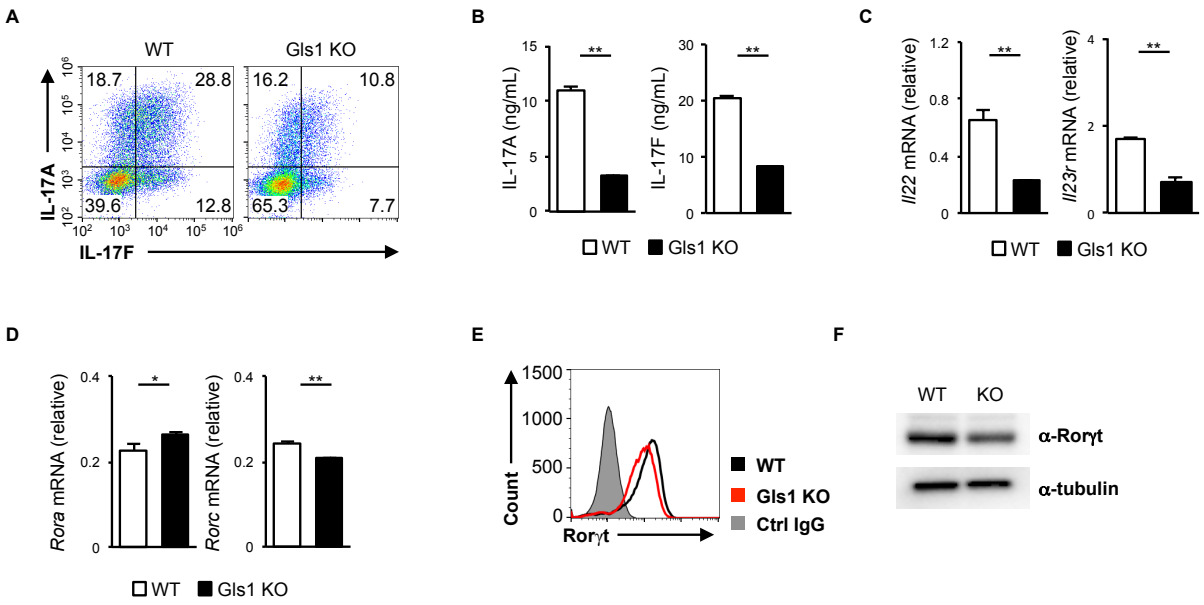

Figure 2 Differentiation of Th17 is selectively impaired in *Gls1*-KO CD4$^+$ T cells

(A) Intracellular staining of IL-17A/IL-17F in WT or *Gls1* KO naive CD4$^+$ T cells cultured under Th17 conditions (IL-6, IL-1β and TGF-β) for day 3. **(B)** Cytokine productions induced Th17 cells in panel (A) were determined by ELISA. **(C)** Quantitative RT-PCR analysis of Th17 cells in panel (A). **(D)** Quantitative RT-PCR analysis of Th17 cells in panel (A). **(E)** Intracellular staining of Rorγt in WT or *Gls1* KO naive CD4$^+$ T cells cultured under Th17 conditions (IL-6, IL-1β and TGF-β) for day 3. **(F)** Immunoblot analysis of Rorγt in WT or *Gls1* KO naive CD4$^+$ T cells cultured under Th17 conditions (IL-6, IL-1β and TGF-β) for day 3. In (B), (C) and (D), all data are expressed as mean of three independent experiments with error bars indicating standard deviation.

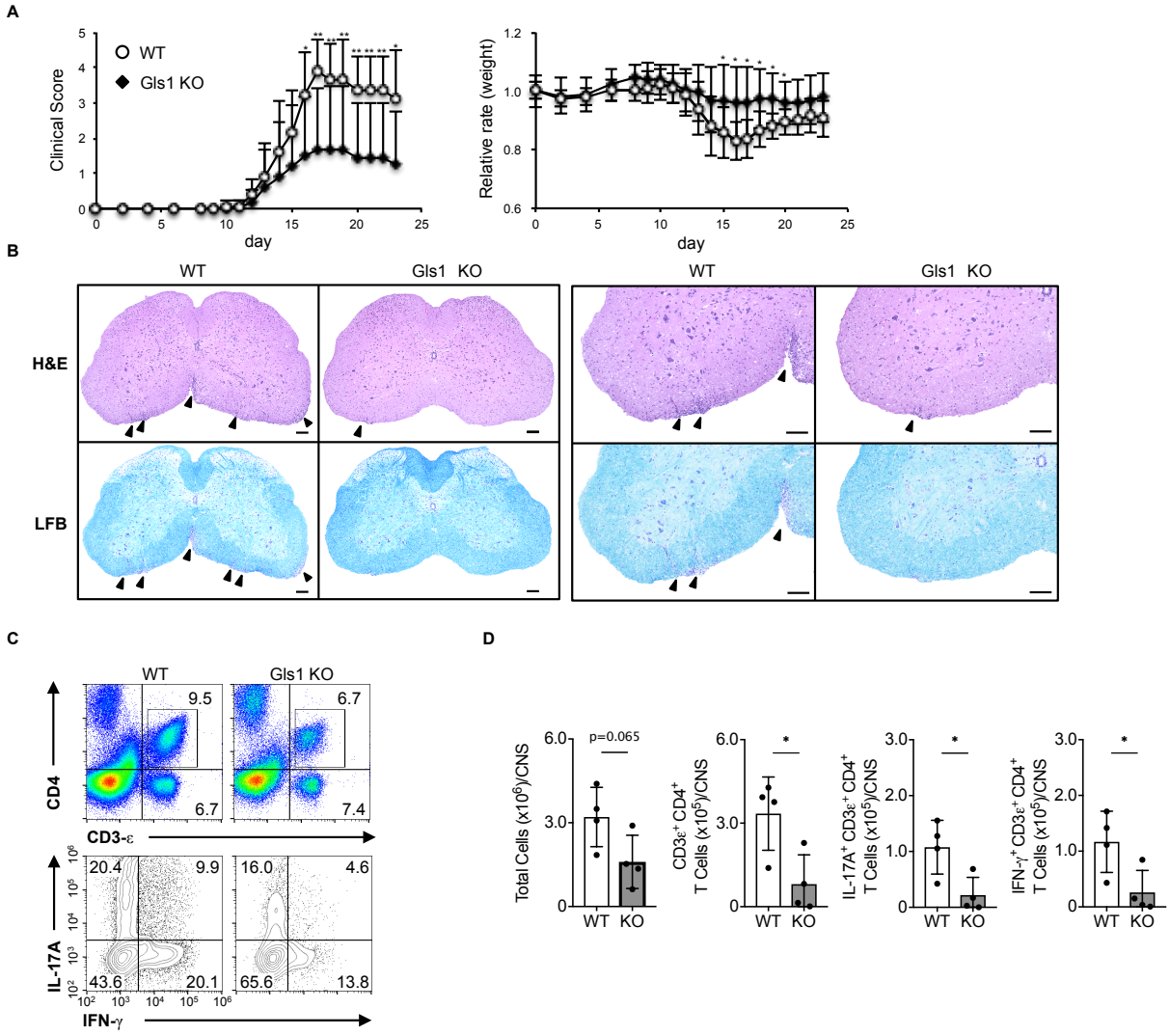

Figure 3 Th17 cell dependent inflammation is ameliorated in T cell-specific *Gls1*-deficient mice

(A) Clinical score and body weight were monitored daily in WT (n=9) and *Gls1* KO (n=10) mice immunized by s.c. with MOG_{35-55} (100 μg/mouse). These data are expressed as mean with error bar indicating standard division. **(B)** Spinal cords were extracted from WT and *Gls1* KO mice at the peak of EAE symptom and stained with Hematoxylin and eosin (H&E) and luxol fast bule (LFB). Inflammatory cells infiltrating central nervus system (CNS) were stained with H&E. Myelin sheath of CNS was stained with LFB. **(C)** Spinal cords were extracted from WT and *Gls1* KO mice at the peak of EAE symptom. Intracellular staining of IL-17A/IFN-γ in $CD3\varepsilon^+$ and $CD4^+$ T cells infiltrating CNS. **(D)** Cell numbers of total cells, $CD4^+$ T cells, IL-17A producing $CD4^+$ T cells and IFN-γ producing $CD4^+$ T cells in spinal cord of WT or *Gls1* KO mice. These data are expressed as individual plots with error bar indicating standard division.

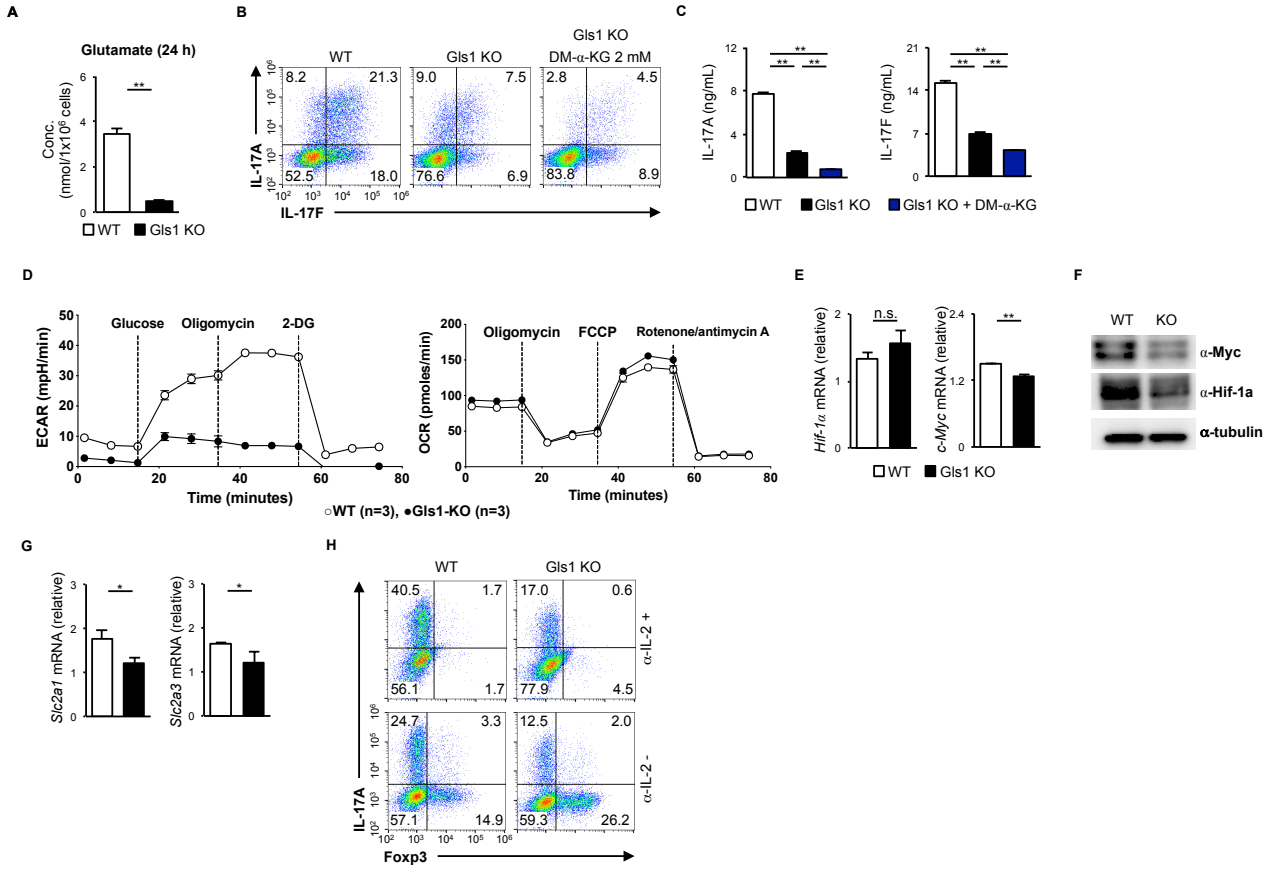

Figure 4 *Gls1*-deficiency suppresses glycolytic activity and alters Th17/Treg balance.

(A) The levels of Intracellular glutamate in WT or *Gls1* KO naive CD4$^+$ T cells stimulated under Th17 conditions. **(B)** Intracellular staining of IL-17A/IL-17F in WT or *Gls1* KO naive CD4$^+$ T cells cultured under Th17 conditions with supplementation of DM-α-KG (2 mM) for day 3. **(C)** Cytokine productions induced Th17 cells in panel (B) were determined by ELISA. **(D)** The results of glycolysis stress test and mito-stress test of Th17 cells in panel (A). **(E)** Quantitative RT-PCR analysis of c-Myc and Hif-1α in Th17 cells in panel (A). **(F)** Immunoblot analysis of c-Myc and Hif-1α in TH17 cells in panel (A). **(G)** Quantitative RT-PCR analysis of scl2a1 and slc2a3 in Th17 cells in panel (A). **(H)** Intracellular staining of IL-17A/IL-17F in WT or Gls1 KO naive CD4+ T cells cultured under Th17 conditions in the presence or absence of neutralizing α-IL-2 mAb for day 3.

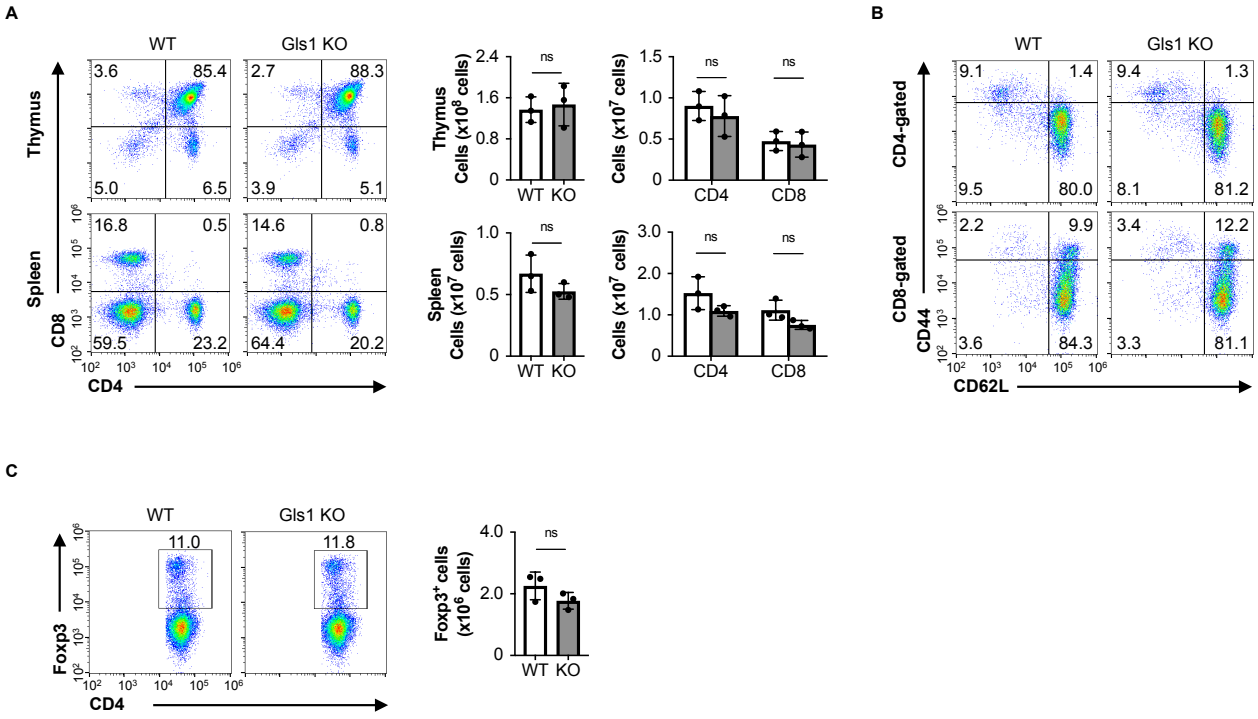

Supplementary Fig. 1 Development and homeostasis of T cells in thymus and spleen in *Gls1*$^{flox/flox}$ x *CD4-Cre* mice.

(A) Surface staining of CD4/CD8 on thymocyte and spleenocyte of WT or *Gls1*$^{flox/flox}$ x *CD4-Cre* mice. Cell numbers of thymocyte and spleenocyte from WT or *Gls1*$^{flox/flox}$ x *CD4-Cre* mice are expressed as individual plots (n = 3) with error bar indicating standard division. **(B)** Surface staining of CD44/CD62L on CD4- or CD8-gated cells in spleenocyte of WT or *Gls1*$^{flox/flox}$ x *CD4-Cre* mice. **(C)** Intracellular staining of Foxp3 in spleenocyte of WT or *Gls1*$^{flox/flox}$ x *CD4-Cre* mice. Cell numbers of Foxp3^{+} CD4^{+} T cells in spleen from WT or *Gls1*$^{flox/flox}$ x *CD4-Cre* mice are expressed as individual plots (n = 3) with error bar indicating standard division.

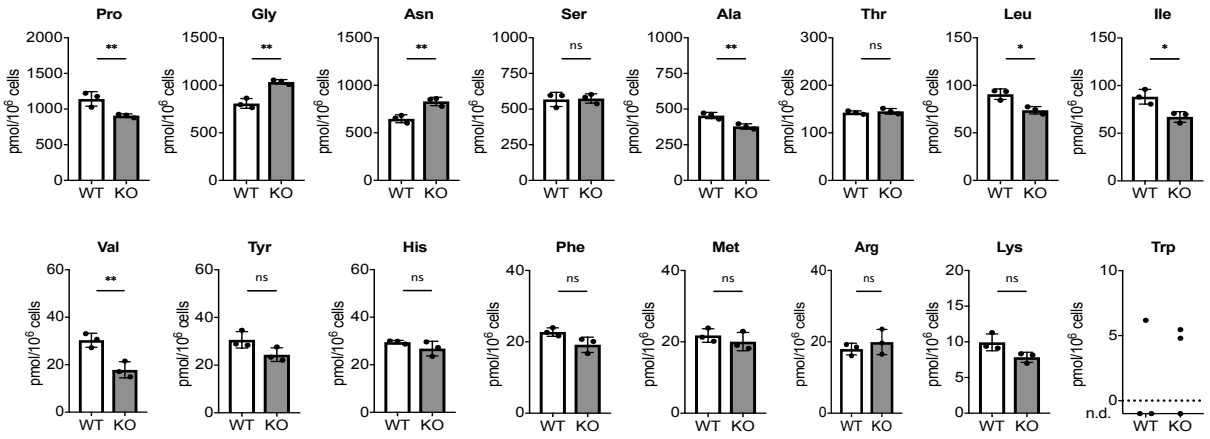

Supplementary Fig. 2 Intracellular levels of amino acids after TCR stimulation.

The intracellular level of amino acids in WT or *Gls1* KO naive $CD4^+$ T cells stimulated with immobilized α-TCR-β mAb plus α-CD28 mAb for 24 h.

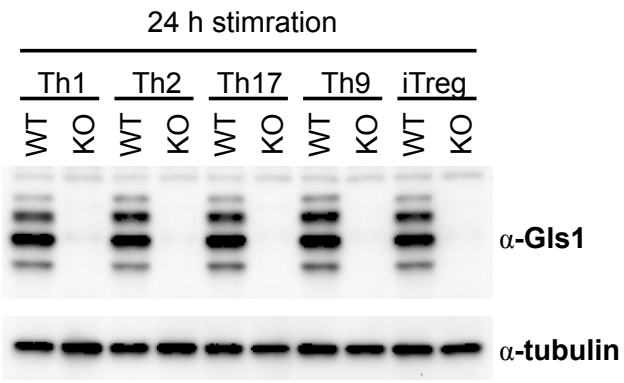

Supplementary Fig. 3 The expression of Gls1 is no difference among Th subsets.

Immunoblot analysis of Gls1 in WT or *Gls1* KO naive $CD4^+$ T cells cultured under each Th subsets conditions for 24 h.

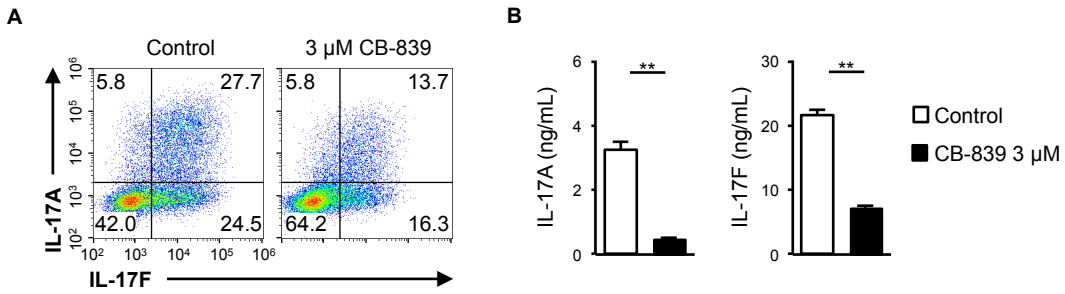

Supplementary Fig. 4 Treatment for Gls1 inhibitor CB-839 during Th17 differentiation.

(A) Intracellular staining of IL-17A/IL-17F in WT naive $CD4^+$ T cells cultured under Th17 conditions in the presence of CB-839 (3 μM) for day 3. **(B)** Cytokine productions induced Th17 cells in panel (A) were determined by ELISA.

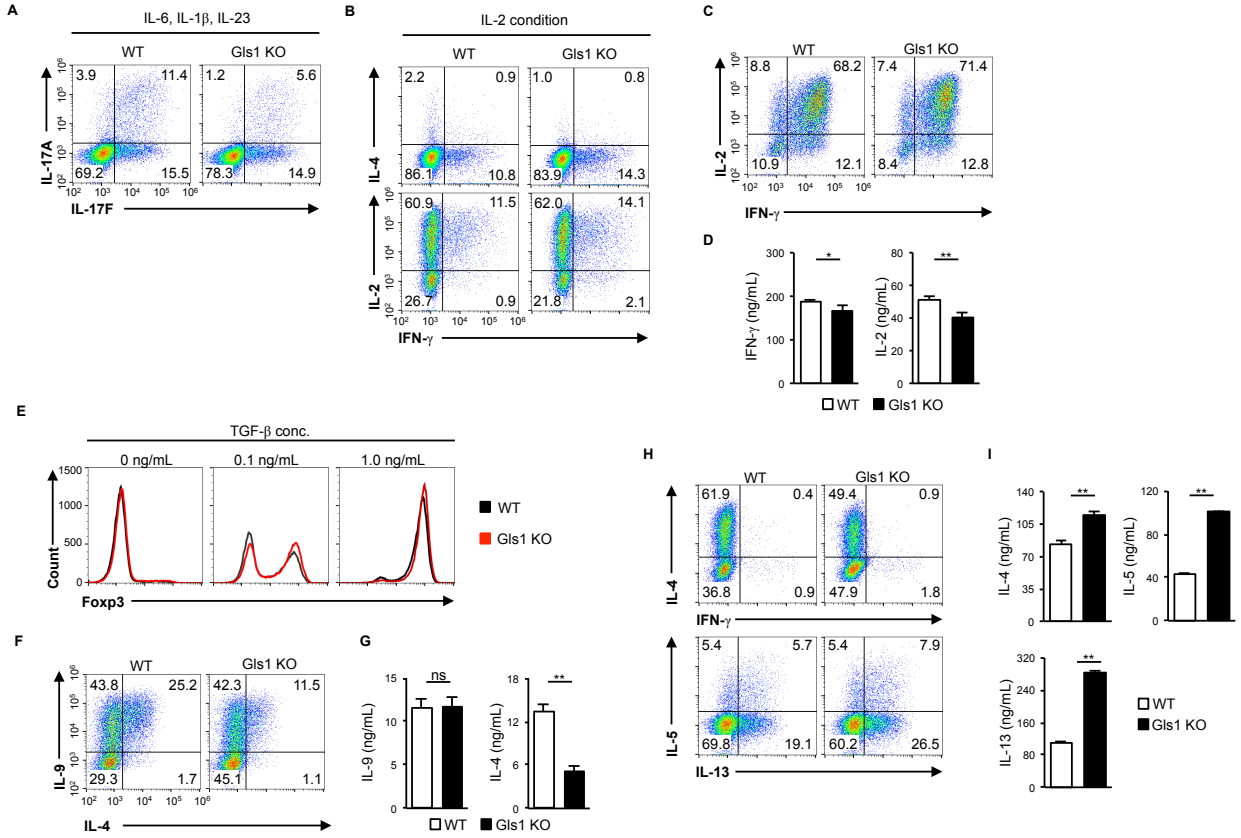

Supplementary Fig. 5 The differentiation of Th subsets in *Gls1* deficient CD4 T cells

(A) Intracellular staining of IL-17A/IL-17F in WT or *Gls1* KO naive $CD4^+$ T cells cultured under pathogenic Th17 conditions (IL-6, IL-1β and IL-23) for day 3. **(B)** Intracellular staining of IL-4/IFN-γ and IL-2/IFN-γ in WT or *Gls1* KO naive $CD4^+$ T cells cultured under IL-2 conditions for day 5. **(C)** Intracellular staining of IL-2/IFN-γ in WT or *Gls1* KO naive $CD4^+$ T cells cultured under Th1 conditions for day 5. **(D)** Cytokine productions induced Th1 cells in panel (C) were determined by ELISA. **(E)** Intracellular staining of Foxp3 in WT or *Gls1* KO naive $CD4^+$ T cells cultured under iTreg conditions for day 3. **(F)** Intracellular staining of IL-9/IL-4 in WT or *Gls1* KO naive $CD4^+$ T cells cultured under Th9 conditions for day 3. **(G)** Cytokine productions induced Th9 cells in panel (F) were determined by ELISA. **(H)** Intracellular staining of IL-4/IFN-γ and IL-5/IL-13 in WT or *Gls1* KO naive $CD4^+$ T cells cultured under Th2 conditions for day 5. **(I)** Cytokine productions induced Th9 cells in panel (H) were determined by ELISA.

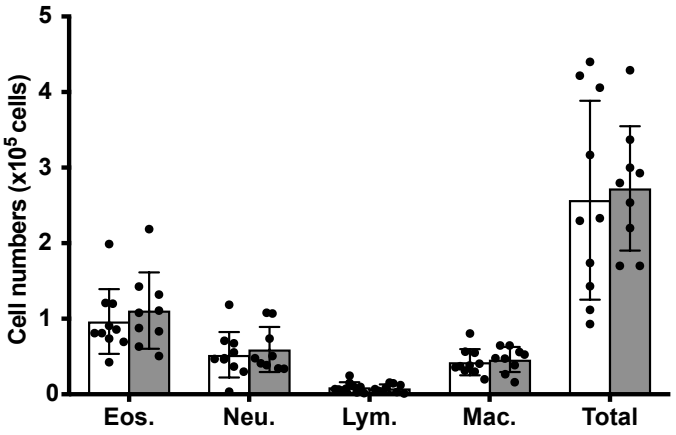

Supplementary Fig. 6

The cell counts of eosinophils (Eos.), neutrophils (Neu.), lymphocytes (Lym.), macrophages (Mac.), and total cells in BAL Fluid of the model mice shown (n = 10 per group). There was no significant difference between the vehicle WT and Gls1-deficient-mice , as detected by ANOVA and Tukey-test.

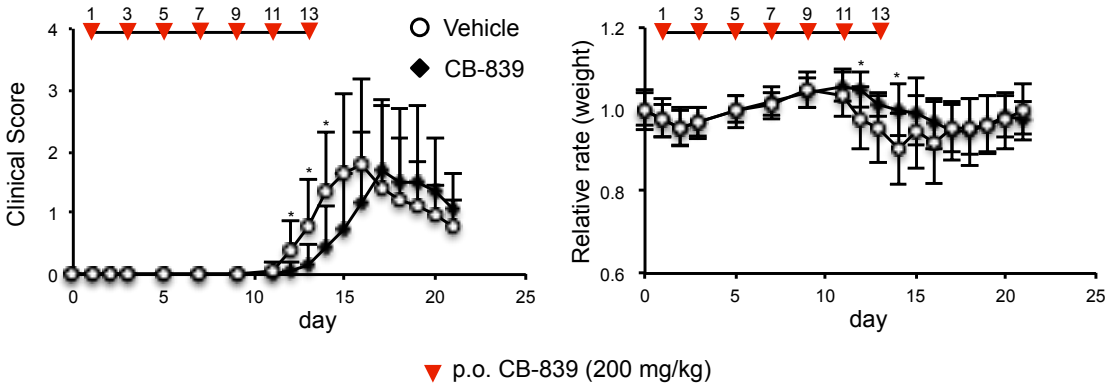

Supplementary Fig. 7 The administration of Gls1 inhibitor CB-839 delayed onset of EAE

Clinical score and body weight were monitored daily in mice immunized by s.c. with MOG_{35-55} (100 μg/mouse). CB-839 was administrated by p.o. (200 mg/kg) on the days showed by red arrows. These data are expressed as mean with error bar indicating standard division.

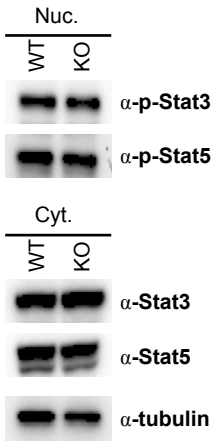

Supplementary Fig. 8 The expression level of total and phospho- Stat3 and Stat5 under Th17 conditions

Immunoblot analysis of total and phospho- Stat3 and Stat5 in WT or *Gls1* KO naive $CD4^+$ T cells cultured under Th17 conditions without neutralizing α-IL-2 mAb for 24 h.

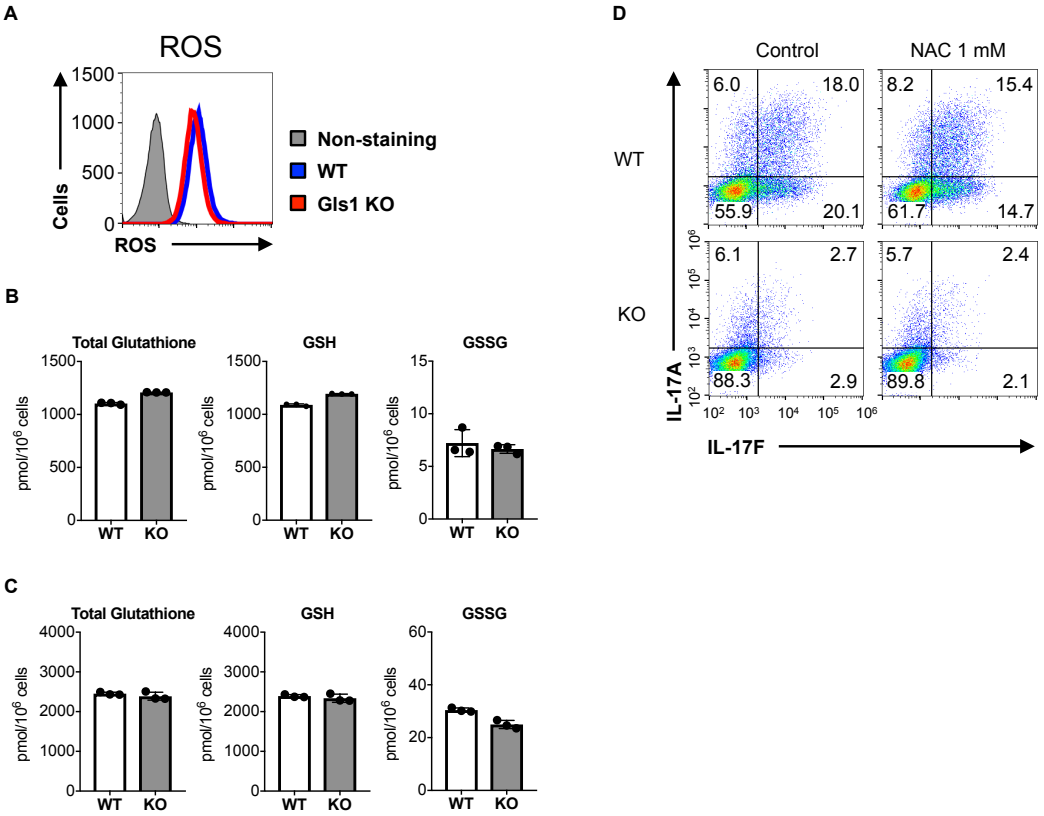

Supplementary Fig. 9 The redox state in *Gls1*-deficient Th17 cells

(A) The levels of Intracellular ROS in WT or *Gls1* KO naive $CD4^+$ T cells stimulated under Th17 conditions. **(B)** The levels of Intracellular glutathione in WT or *Gls1* KO naive $CD4^+$ T cells stimulated under Th17 conditions for 24 h. **(C)** The levels of Intracellular glutathione in WT or *Gls1* KO naive $CD4^+$ T cells stimulated under Th17 conditions for 48 h. **(D)** Intracellular staining of IL-17A/IL-17F in WT or *Gls1* KO naive $CD4^+$ T cells cultured under Th17 conditions with supplementation of NAC (1 mM) for day 3.

Table

Regent	Resouce	Identifier	
Material used for cell cluture			
Recobinant mouse IL-6	FUJIFILM Wako Pure Chemical Corporation	Cat# 093-04433	
Recobinant mouse IL-1 β	FUJIFILM Wako Pure Chemical Corporation	Cat# 094-04681	
Recombinant human TGF- β 1	R&D systems	Cat# 240-B-002	
Recombinant mouse IL-2	TONBO Biosciences	Cat# 21-8021	
Recombinant mouse IL-4	Peprotech	Cat# 214-14	
Recombinant mouse IL-12 p70	Peprotech	Cat# 210-12	
Recombinant mouse IL-23	R&D systems	Cat# 1887-ML	
Ultra-LEAF™ Purified anti-mouse CD28 mAb (clone 37.51)	BioLegend	Cat# 102116	
Ultra-LEAF™ Purified anti-mouse IFN- γ mAb (clone XMG1.2)	BioLegend	Cat# 505834	
Ultra-LEAF™ Purified anti-mouse IL-4 mAb (clone 11B11)	BioLegend	Cat# 504122	
LEAF Purified anti-mouse IL-2 antibody (clone JES6-1A12)	BioLegend	Cat# 503704	
anti-mouse IL-10 (clone JES5-16E3)	BD Biosciences	Cat# 554463	
Material used for ELISA			
Mouse IL-17A DuoSet ELISA	R&D system	Cat# DY421	
Mouse IL-17F DuoSet ELISA	R&D system	Cat# DY2057	
Mouse IL-13 Duoset ELISA	R&D system	Cat# DY413	
Mouse TNF- α DuoSet ELISA	R&D system	Cat# DY410	
DuoSet Ancillary Reagent Kit 2	R&D system	Cat# DY008	
ELISA MAX™ Deluxe Set Mouse IL-9	BioLegend	Cat# 442704	
anti-mouse IL-4 Rat capture mAb (clone BVD4-1D11)	BD Bioscienses	Cat# 554387	
Biotin anti-mouse IL-4 Rat detection mAb (clone BVD6-24G2)	BD Bioscienses	Cat# 554390	
recombinant mouse IL-4	Peprotech	Cat# 214-14	
anti-mouse/human IL-5 Rat capture mAb (clone TRFK5)	BD Bioscienses	Cat# 554393	
Biotin anti-mouse IL-5 Rat detection mAb (clone TRK4)	BD Bioscienses	Cat# 554397	
recombinant mouse IL-5 (ELISA Std.)	BioLegend	Cat# 576709	
anti-mouse IFN- γ Rat capture mAb (clone R4-6A2)	BD Bioscienses	Cat# 551216	
Biotin anti-mouse IFN- γ Rat detection mAb (clone XMG1.2)	BD Bioscienses	Cat# 554410	
recombinant mouse IFN- γ	Peprotech	Cat# 315-05	
anti-mouse IL-2 Rat capture mAb (clone JES6-1A12)	BD Bioscienses	Cat# 554424	
Biotin anti-mouse IL-2 Rat detection mAb (clone JES6-5H4)	BD Bioscienses	Cat# 554426	
recombinant mouse IL-2	Peprotech	Cat# 212-12	
Streptavidin-HRP	Invitrogen	Cat# 434323	
TMB peroxidase EIA substrate kit	Bio-RAD	Cat#1721066	
Material using for I.B.			
anti-Gls1 (KGA/GAC) Rabbit pAb (clone AG3505)	Proteintech	Cat# 12855-1-AP	1:1000
anti-Ror γ t Rat mAb (clone B2D)	eBioscience	Cat# 14-6981-80	1:500
anti-HIF1- α Rabbit pAb	BETHYL	Cat# A300-286A	1:2000
anit-c-Myc Rabbit mAb (clone D84C12)	Cell signaling technology	Cat# 5605	1:1000
anti- α -tubulin Rabbit mAb (clone 11H10)	Cell signaling technology	Cat# 2125	1:2000
anti-Rabbit IgG, HRP-Linked Whole Ab Donkey	GE Healthcare	Cat# NA934	1:5000
anti-Mouse IgG, HRP-Linked Whole Ab Sheep	GE Healthcare	Cat# NA931	1:4000
anti-Rat IgG (H+L), HRP Goat	Southern Biotech	Cat# 3050-05	1:5000
Amersham Hybond P PVDF 0.45 (300 mm × 4 m)	GE Healthcare	Cat# 10600023	
Clarity Western ECL Substrate	BioRad	Cat# 1705061	
ChemiDoc XRS Plus	BioRad		
Antibody used for FACS			
anti-mouse CD3 ε -FITC (clone 145-2C11)	BD Bioscience	Cat# 553062	1:30
anti-mouse CD4-FITC (clone RM4-5)	BD Bioscience	Cat# 553047	1:100
anti-mouse CD62L-APC (clone MEL-14)	TONBO Biosciences	Cat# 20-0261-U100	1:100
anti-mouse/human CD44-PE (clone IM7)	TONBO Biosciences	Cat# 50-0441-U100	1:100
anti-mouse CD4-APCCy7 (clone RM4-5)	BioLegend	Cat# 100525	1:100
anti-mouse IL-17A-PE (clone TC11-18H10.1)	BioLegend	Cat# 506904	1:50
anti-mouse IL-17F-Alexa Fluor 647 (clone 9D3.1C8)	BioLegend	Cat# 517004	1:50
anti-mouse IFN- γ -FITC (clone XMG1.2)	BD Bioscience	Cat# 554411	1:500
anti-mouse IL-2-APC (clone JES6-5H4)	BD Bioscience	Cat# 554429	1:50
anti-mouse IL-4-PE antibody (clone 11B11)	BioLegend	Cat# 504103	1:50
anti-mouse IL-4-APC (clone 11B11)	BD Bioscience	Cat# 554436	1:50
anti-mouse/human IL-5-APC antibody (clone TRFK5)	BioLegend	Cat# 504305	1:50
anti-mouse IL-13-PE (clone eBip13A)	eBioscience	Cat# 12-7133-82	1:30
anti-mouse IL-9-PE (clone RM9A4)	BioLegend	Cat# 514103	1:50
anti-mouse/rat/human FOXP3-Alexa647 (clone 150D)	BioLegend	Cat# 320013	2.5 μL/1.0x10^6 cells
anti-rabbit phospho-4e-bp1 (Thr37/46)-Alexa Fluor 488 mAb (clone 236B4)	Cell signaling technology	Cat# 2846	1 μL/1.0x10^6 cells
anti-rabbit phospho-S6 ribosomal protein (Ser235/236)-Alexa Fluor 647 mAb (clone D57.2.2E)	Cell signaling technology	Cat# 4851	1 μL/1.0x10^6 cells
anti-rabbit phospho-S6 ribosomal protein (Ser240/244)-AlexaFluor 647 mAb	Cell signaling technology	Cat# 5044	1 μL/1.0x10^6 cells

Acknowledgment

I wish to express my most sincere gratitude to Professor Tatsuya Sawasaki and Professor Masakatsu Yamashita for useful comments, remarks and encouragement throughout process this thesis. They continually and convincingly conveyed a spit of adventure and an excitement in regard to research. Without his guidance and persistent help this dissertation would not have been possible.

I would like to thank Senior Assistant Professor Hirotaka Takahashi, Senior Assistant Professor Makoto Kuwahara, Assistant Professor Jupei Suzuki for their guidance, valuable discussions and encouragement.

I would also like to thank my mentorship of Mr. Satoshi Yamanaka and Mr. Kohki Kido for their guidance, valuable discussions and persistent help.

I thank all laboratory members of Proteo-Science Center (PROS), Ehime University.
I thank all laboratory members of Department of Immunology, Graduate School of Medicine, Ehime University.

I thank the members of Advanced Research Support Center (ADRES), Ehime University.
This work was supported by a Grant-in-Aid for JSPS Fellows from Japan Society for Promotion of Science.

Finally, I wish to express my deepest gratitude to my family for supports throughout my student life.